ARTICLE

Phosphate has dual roles in cross-bridge kinetics in rabbit psoas single myofibrils

Masataka Kawai[1], Robert Stehle[2], Gabriele Pfitzer[2,3], and Bogdan Iorga[2,4,5]

In this study, we aimed to study the role of inorganic phosphate (P_i) in the production of oscillatory work and cross-bridge (CB) kinetics of striated muscle. We applied small-amplitude sinusoidal length oscillations to rabbit psoas single myofibrils and muscle fibers, and the resulting force responses were analyzed during maximal Ca^{2+} activation (pCa 4.65) at 15°C. Three exponential processes, A, B, and C, were identified from the tension transients, which were studied as functions of P_i concentration ($[P_i]$). In myofibrils, we found that process C, corresponding to phase 2 of step analysis during isometric contraction, is almost a perfect single exponential function compared with skinned fibers, which exhibit distributed rate constants, as described previously. The $[P_i]$ dependence of the apparent rate constants $2\pi b$ and $2\pi c$, and that of isometric tension, was studied to characterize the force generation and P_i release steps in the CB cycle, as well as the inhibitory effect of P_i. In contrast to skinned fibers, P_i does not accumulate in the core of myofibrils, allowing sinusoidal analysis to be performed nearly at $[P_i]$ = 0. Process B disappeared as $[P_i]$ approached 0 mM in myofibrils, indicating the significance of the role of P_i rebinding to CBs in the production of oscillatory work (process B). Our results also suggest that P_i competitively inhibits ATP binding to CBs, with an inhibitory dissociation constant of ~2.6 mM. Finally, we found that the sinusoidal waveform of tension is mostly distorted by second harmonics and that this distortion is closely correlated with production of oscillatory work, indicating that the mechanism of generating force is intrinsically nonlinear. A nonlinear force generation mechanism suggests that the length-dependent intrinsic rate constant is asymmetric upon stretch and release and that there may be a ratchet mechanism involved in the CB cycle.

Introduction

There has been a great deal of discussion about the role of P_i in the cross-bridge (CB) kinetics of striated muscle contraction. Our study is aimed at testing the role of P_i in oscillatory work production (also called exponential process B) and its relationship to force generation. Oscillatory work is typically seen in insect flight muscles (Pringle, 1967). Isometrically contracting fast-twitch mammalian skeletal muscles can also perform oscillatory work on the oscillating length driver (Kawai and Brandt, 1980; Galler et al., 2005), transducing chemical energy from ATP hydrolysis (Rüegg and Tregear, 1966). The exponential process B corresponds to delayed tension or phase 3 in step analysis, as previously demonstrated (Kawai and Brandt, 1980). The relationship between "processes" in sinusoidal analysis and "phases" in step analysis is summarized in Table 1. This table also includes the estimates of the rate constants measured from length transient analysis (Caremani et al., 2013), although

correlation of tension transients and length transients is not straightforward. The general rule is that a fast process in one method corresponds to a fast process in the other, but the correlation becomes weaker as the process becomes slower. It is thought that oscillatory work provides signals from the step that generates force, because, at this frequency, work is performed on the forcing apparatus (length driver), and oscillatory work and the ATP hydrolysis rate are well correlated (Rüegg and Tregear, 1966). Our method uses single myofibrils (see Fig. 1 in Iorga et al., 2012), a subcellular structure of striated muscle cells, in which tension and its transients can be measured during Ca^{2+} activation. The advantage of working with myofibrils is that there is little diffusion barrier between the interior of the preparation and the bathing medium; thus, the concentration of an ionic species in the myofilament lattice space can be more accurately defined and its difference can be reduced below

[1]Department of Anatomy and Cell Biology, University of Iowa, Iowa City, IA; [2]Institute of Vegetative Physiology, University of Köln, Köln, Germany; [3]Institute of Neurophysiology, University of Köln, Köln, Germany; [4]Department of Molecular and Cell Physiology, Hannover Medical School, Hannover, Germany; [5]Department of Physical Chemistry, Faculty of Chemistry, University of Bucharest, Bucharest, Romania.

Correspondence to Masataka Kawai: masataka-kawai@uiowa.edu

This work is part of a special collection on myofilament function and disease.

Table 1. **Correlations in transient analysis methods using tension/length transients**

Methods	Slow	Intermediate	Fast	Very fast
Sinusoidal analysis	Process A	Process B	Process C	Y_∞
(Tension transients)		Oscillatory work		
	Phase advance	Phase delay	Phase advance	
Isometric step	Phase 4	Phase 3	Phase 2	Phase 1
(Tension transients)		Delayed tension		
	Exponential advance	Exponential delay	Exponential advance	
Isotonic step (length transients)	Steady velocity of shortening phase	Phase 3 with the rate constant r_3	Phase 2 with the rate constant r_2	Phase 1
Mechanisms in CB cycle	Step 6 (linear work production)	Step 4 (force generation, oscillatory work production)	Step 2 (CB detachment after ATP binding)	

The correlation between processes in sinusoidal analysis and phases in step analysis is theoretically perfect (Kawai and Brandt, 1980), and the measurements are carried out under the isometric condition. The correlation between tension transients and length transients is only approximate. The general rule is that a fast process in one method corresponds to a fast process in the other, but the correlation becomes weaker as the process becomes slower. The polarity of process A (phase 4) and process C (phase 2) is positive, and the polarity of process B (phase 3) is negative (Eq. 4). For the length transients, terminology used previously (Caremani et al., 2013) is employed.

0.01 mM (Tesi et al., 2000). This is in contrast to skinned muscle fibers, where up to a 2-mM difference in ATP, ADP, and P_i concentrations is predicted in the core of fibers, even in the presence of an ATP regenerating system (Cooke and Pate, 1985). When no P_i is added to experimental saline, the actual $[P_i]$ in psoas fibers is estimated to be ~0.7–0.8 mM during maximal activation at 20°C (Kawai and Halvorson, 1991; Dantzig et al., 1992). Like muscle fibers, myofibrils enable the measurement of force, which is an indispensable feature for studying chemomechanical transduction. We employ a small-amplitude, sinusoidal length perturbation method (≤0.2% of muscle length) at varying frequencies, which is highly effective for resolving the elementary step of the CB cycle (Kawai and Halvorson, 2007). In this study, we examine the effect of P_i on force transients of isometrically contracting myofibrils to characterize the elementary steps of the CB cycle more accurately.

The use of myofibrils from vertebrate skeletal muscles started in the mid-1980s. Sugi et al. (1983) used split fibers, which were large bundles of myofibrils. Bartoo et al. (1993) used small bundles of myofibrils and reported isometric tension as large as 590 kPa, whereas the typical tension developed by single fibers is ~200 kPa. Bartoo et al. argued that this difference in tension

was caused by the concentration gradient of Ca^{2+} and ATP. In other studies (Tesi et al., 2002), researchers used myofibrils and reported that tension diminished by P_i is larger than that reported for muscle fibers. They argued that the difference is caused by the concentration gradient of P_i in fibers. They further studied transients caused by a sudden increase in $[P_i]$ and observed a rapid tension decay (Tesi et al., 2000), similar to that in caged-P_i studies (e.g., Dantzig et al., 1992).

However, using cardiac myofibrils, Stehle (2017) reported that sarcomere inhomogeneity and wave propagation (sarcomere dynamics) occurred during P_i-induced rapid tension decay. This phenomenon is reminiscent of sudden sarcomere elongation in frog semitendinosus intact muscle fibers (Kawai, 1971) and heterogeneous sarcomere length (SL) in myofibrils during relaxation (Stehle et al., 2002b; Poggesi et al., 2005). Upon Ca^{2+} removal, thin filaments are turned off, together with the cooperative activation mechanisms. This process is not simultaneous along the length of the fibers, and heterogeneous contraction/relaxation occurs at the level of each sarcomere. Tesi et al. (2000) and later Stehle (2017) studied a sudden decrease in the $[P_i]$, and both observed that the rate constant k_{-Pi} of the transient was slower than the rate constant k_{+Pi} after a sudden increase in the $[P_i]$. The rate constant k_{-Pi} was similar to k_{TR} (rate constant of tension redevelopment) that is measured following a sudden transition from an isotonic (mechanically unloaded) to isometric (mechanically loaded) contraction. This experiment was applied to Ca^{2+}-activated, isometrically held myofibrils or muscle fibers, and the duration of the length release was 10–20% before the myofibrils (or fibers) quickly stretched back to their initial length (Brenner, 1988). It was thought that the Ca^{2+}-induced tension development time course was limited by a slow process during the CB cycle that also limited the rate of k_{TR} (Gordon et al., 2000; Wang and Kawai, 2013).

To characterize the elementary steps of the CB cycle, we have employed a method that causes small sinusoidal length changes, and we recorded concomitant amplitude and phase shift in tension. These are tension transients. The preparation is held almost isometric, and this method does not cause heterogeneous sarcomere contractions (Iorga et al., 2012). Because of this, the activated myofibrils are not mechanically unloaded; therefore, a sudden change in the mechanical conditions (such as from isometric to isotonic and then back to isometric) does not occur. Because the myofibril preparation is already in tension, series elastic elements (Huxley et al., 1994; Wakabayashi et al., 1994; Higuchi et al., 1995) are stretched to their full extent. Without this level of tension, the series elastic elements might decrease the time course and complicate interpretations. During the tension plateau, no further change in the SL or the regulatory state of thin filaments was seen (Iorga et al., 2012). The typical amplitude of the length change (L_1) is 0.2% of the length of the preparation (L_0), which corresponds to 2.5 nm/half sarcomere (1.25 μm × 0.2%) when the SL is 2.5 μm (skeletal myofibrils). Because of the presence of series compliance, it is estimated that one-half (~1.3 nm) of this change is applied to each CB under our standard Ca^{2+}-activating conditions (Kawai, 2003). It is essential that this value be kept less than the myosin step size (5.3–12 nm)

or power stroke so that transients associated with the elementary steps of the CB cycle can be resolved. By choosing the frequency, we can make the length oscillation resonate to an elementary chemical step of the CB cycle, thereby maximizing the signal from the particular elementary step. The signal-to-noise ratio can be improved by averaging the signals of many sinusoidal cycles.

In this study, we apply the sinusoidal analysis method to explore the dependence of elementary steps on $[P_i]$ in Ca^{2+}-activated rabbit psoas myofibrils and compared the results with those from muscle fibers. One major advantage of working with myofibrils over fibers is the short diffusion distance, which ensures rapid equilibration of the saline in the sarcomere with the surrounding solution. Unlike fibers, there is little accumulation of P_i or ADP caused by ATP hydrolysis in the preparation. This characteristic enabled us to explore force response to sinusoidal length changes, essentially in the absence of P_i binding to CBs. We found that under this condition, the magnitude of oscillatory work was reduced to nearly zero, as assumed earlier (Kawai and Halvorson, 1991). The effect observed in myofibrils at a low $[P_i]$ demonstrates that P_i binding is a major determinant of the oscillatory work described in sinusoidal analysis and delayed tension (phase 3) in step analysis of isometric contraction. The results are discussed in terms of the CB model, in which the reverse transition of CBs from force- to non–force-generating states is coupled to P_i binding, which generates the oscillatory work. Our results suggest that P_i may also competitively inhibit the ATP binding to the myosin head.

Materials and methods

Myofibril studies were performed at the Institute of Vegetative Physiology, University of Köln, and muscle fiber studies were performed at the Department of Anatomy and Cell Biology, University of Iowa. All animal studies were conducted in accordance with institutional guidelines and approved by the animal research committees at the University of Köln and the University of Iowa. The University of Iowa has an Animal Welfare Assurance (A-3021-01) on file with the Office of Laboratory Animal Welfare, National Institutes of Health.

Myofibril preparations
The myofibril preparations were as previously described (Iorga et al., 2012). In brief, muscle bundles from rabbit psoas were tied to a wooden stick and incubated, first in Na-skinning solution for 1–2 h and then in K-skinning solution for another 1–2 h, in the presence of protease inhibitors and 2 mM dithiothreitol at 0–4°C. Muscle bundles were equilibrated in K-skinning solution mixed with 50% (vol/vol) glycerol for ~6 h and then transferred to a freezer (−20°C), where they were kept for <1 mo without freezing. For myofibril preparations, a small segment was removed from a stored bundle, homogenized using a T8 Ultra-Turrax tissue homogenizer (IKA Works) at 25,000 rpm for 5–7 s, and filtered through a 22-μm polypropylene mesh to remove large myofibril bundles. A small volume of the suspension was transferred to a temperature-controlled experimental chamber, where myofibrils were sedimented for ~1 h in the relaxing solution. Thin

myofibril bundles, consisting of two to four myofibrils, were selected and mounted between a needle connected to the length driver and the tip of the force transducer.

The SL of the myofibril preparation was initially adjusted to 2.7 μm in the relaxing solution by using a video monitor. The preparation was taut (bow shaped) because of the flow of the solution caused by gravitational force. Upon generation of a force, the preparation became straight with an SL of ~2.5 μm, which is at the peak of the length–tension diagram in rabbit psoas preparations (Higuchi et al., 1995); sarcomere shortening in rabbit psoas myofibrils is the most homogeneous at SL of 2.0–2.6 μm (Bartoo et al., 1993). The diameter and length of the myofibrils were determined from the video monitor. This type of preparation develops ~0.5 μN of force in the activating solution. At the beginning and end of the experimental series, the myofibril preparation was tested with the standard activating solution, and reproducibility of the data was examined. Data from any preparation that exhibited ≤80% force were not used for analysis. The details of the rabbit psoas myofibril preparation were previously described (Knight and Trinick, 1982; Bartoo et al., 1993; Colomo et al., 1997; Stehle et al., 2002b; Rassier et al., 2003; Iorga et al., 2012).

Experimental apparatus to study myofibril mechanics
For this part of the experiments, performed at the University of Köln, the experimental apparatus was built on an Olympus IX70 inverted microscope, as described previously (Stehle et al., 2002a; Stehle et al., 2002b). In brief, a rectangular muscle chamber (with clear windows on the sides and bottom) was placed on the microscope stage. The temperature was regulated to 15°C. On the left, a micromanipulator held a piezoactuator (P-821.20; Physik Instruments), which served as the length driver, and its moving end was connected to a microtool, a tungsten needle. On the right, the micromanipulator held a cantilever (Nanosensors) used for atomic force microscopy. The beam of a 4-mW diode laser (660 nm) was focused onto the cantilever (resonance, ~60 kHz), and the reflected light was sensed as the difference in two currents by a double-photodiode detector. This signal was used as the force signal. The myofibrils were glued to these moving parts using a 1:3 mixture of silicon glue (3140 RTV Coating; Dow Corning) and 2% nitrocellulose dissolved in amyl acetate (Stehle et al., 2002a). The typical length (L_0) of a preparation was 50–60 μm, and the diameter was 2–3 μm.

A series of syringes containing experimental solutions was suspended 300 mm above the experimental chamber, and each solution was injected by using gravitational force through chromatography tubing that opened 500 μm ahead of the myofibrils. The experimental solution flowed past the myofibrils at a rate of ~50 mm/s (Tesi et al., 2002). Different solutions were injected by operating solution switches, the outputs of which were merged into two chromatography tubes. These were channeled into openings of a θ capillary (TGC150-15; Clark Electromedical Instruments), and solutions were switched by quickly shifting the θ capillary using a piezoactuator (P289.40; Physik Instruments; Colomo et al., 1998; Poggesi et al., 2005).

The frequency range of this apparatus was limited between 1 and 250 Hz. Working with a lower frequency range (<1 Hz) was not practical, because a significant amount of time was required

to produce at least one sine cycle, resulting in a slow drift of the tension baseline. An extended period of time can also deteriorate the preparation and lead to problems. The frequency range of the apparatus was adequate to characterize processes B and C, which are the major subjects of the present report. By measuring isometric tension before and after sinusoidal length oscillation at each frequency, the drift was detrended, but the detrending was not perfect. For a typical time course record of myofibril experiments, see Fig. S1.

Muscle fiber experiments

For this part of the experiments, performed at the University of Iowa, bundles of rabbit psoas fibers were prepared as described previously (Zhao et al., 1996) and stored at –20°C in the storage solution. Single fibers were dissected and mounted to the experimental apparatus. One end of the preparation was glued (using nail polish) to the length driver as described previously (Kawai and Brandt, 1980). The other end was glued to the tip of a Güth-type force transducer (Myotronic UG). The length of the preparation (L_O) was 3–4 mm with a diameter of 60–100 μm. SL was adjusted to 2.5 μm by optical diffraction using an He-Ne laser. The solution was changed by vacuum, and new solution was injected using a 500-μl pipette. The detailed experimental methods were described previously (Kawai and Brandt, 1980). Data were collected up to 250 Hz, but the data between 130 and 250 Hz were contaminated with artifacts (resonance of tension transducer, poor rigor response used to correct instrument response, etc.); therefore, data collected at ≤100 Hz were used for analyses. The frequency range of 0.25–100 Hz is adequate to characterize all three exponential processes because the peak viscose modulus (or phase shift) is within this range, as seen in Figs. 2 and 3. The rabbit psoas is a fast-twitch type IID muscle (Galler et al., 2005). A typical muscle fiber experiment is shown in Fig. S2.

Sinusoidal analysis

During the tension plateau, the length of the preparations (myofibrils or skinned muscle fibers) was oscillated with small-amplitude sinewaves in the frequency ranges of 1–250 Hz (corresponding time domain, 0.64–160 ms) for myofibrils and 0.25–100 Hz (0.64–640 ms) for muscle fibers. The amplitude of the oscillations was 0.125% (fibers) or 0.2% L_O (myofibrils), which corresponds to ±0.8–1.1 nm at the CB level, assuming 50% series compliance as suggested previously (Kawai, 2003). As the steady state is achieved in 0.25 s, n pairs of length time course (l_1, l_2,...l_n) and force time course (f_1, f_2,...f_n) were collected and analyzed in terms of the discrete Fourier transform, as described previously (Kawai, 2018). These are functions of frequency (ν). With proper normalization for the length (L_O) and the cross-sectional area of the preparation, we used strain and stress (tension) in place of length and force, respectively. The length signal is expanded in Fourier series:

$$L_k(\nu) = \frac{1}{n} \sum_{j=1}^{n} l_j \exp\left(-\frac{2\pi jk}{n}i\right), \qquad (1)$$

where $i = \sqrt{-1}$ and $k = 1, 2,...n$. In myofibrils, the paired data (length and force) were collected at the rate of 2,000 points/s,

resulting in 80,000 data points in the record of 20 s, such as shown in Fig. S1. In muscle fibers, two 16-bit A/D converters were run at the speed of 100,000 points/s, but the data were reduced to 20–40 data pairs in each sine cycle by the data collection program Dcoll.EXE (homemade), resulting in 1,040 data points to obtain one frequency-dependent complex modulus function $Y(\nu)$ (Kawai and Brandt, 1980; Kawai, 2018). We set $L_1 = |L_1|$ (real number) as the amplitude of the length oscillation, and we set L_2, L_3,...L_{n-1} = 0, because the driving signal is a pure sinewave. $L_n = L_0$ is the length of the preparation. The force signal is also expanded in the Fourier series:

$$F_k(\nu) = \frac{1}{n} \sum_{j=1}^{n} f_j \exp\left(-\frac{2\pi jk}{n}i\right) \qquad (2)$$

and

$$Y_k(\nu) = \frac{F_k(\nu)}{L_1}, \qquad (3)$$

where $F_k(\nu)$ is the kth-order harmonic component (amplitude and phase) of force and $Y_k(\nu)$ is the kth-order complex modulus. The complex modulus we have used for publications in the past is its first order: $Y(\nu) = Y_1(\nu)$. The real part of this quantity [Re $Y(\nu)$] is the elastic modulus; the imaginary part [Im $Y(\nu)$] is the viscous modulus; the absolute value ($|Y(\nu)|$) is the dynamic modulus; and the phase [Arg $Y(\nu)$] is the phase shift. $F_n = F_O$ is the average tension over n points.

The complex modulus data [$Y_k(\nu)$] are fitted to Eq. 4, which consists of three exponential processes (Kawai et al., 1977), processes A, B, and C:

$$Y(\nu) = H + \frac{A\nu i}{a + \nu i} - \frac{B\nu i}{b + \nu i} + \frac{C\nu i}{c + \nu i}. \qquad (4)$$

a, b, and c are the characteristic frequencies ($0 < a < b < c$) of processes A, B, and C, respectively, and A, B, and C (all positive numbers) are their respective magnitudes (amplitudes). $2\pi a$, $2\pi b$, and $2\pi c$ correspond to their respective apparent (measured) rate constants. Y_∞ (= $H + A - B + C$) is the elastic modulus extrapolated to the infinite frequency (∞) and is often called "stiffness" in muscle mechanics literature. Process B has a negative sign in Eq. 4 because, at around the frequency b, the phase shift has a negative value (Fig. 3, B and D), and the dynamic modulus has a local minimum: a dip frequency called ν_{min} (or f_{min}) at ~10–30 Hz for fast-twitch skeletal muscle fibers (Fig. 3 C) and myofibrils (Fig. 3 A). The muscle preparations generate oscillatory work on the forcing apparatus (length driver) at around frequency b. $b < \nu_{min} < c$, where ν_{min} is closer to b than to c. The oscillatory work is the same component known as phase 3 in step analysis (Heinl et al., 1974; Huxley, 1974; see Table 1 for their correlation). In step analysis, it is represented as a delayed rise in tension when the muscle is stretched and a delayed decay in tension when the muscle is released. The oscillatory work is also known as process B in sinusoidal analyses (Kawai et al., 1977; Kawai, 1978; Kawai and Brandt, 1980). Each of these three processes is called an exponential, because their time domain expression consists of exponential functions. The processes A, B, and C, respectively, correspond to phases 4, 3, and 2,

and Y_∞ corresponds to phase 1 of step analysis (Table 1; Heinl et al., 1974; Huxley, 1974). The complex modulus data from myofibrils and muscle fibers were corrected by using the complex modulus derived from myofibrils in rigor and muscle fibers in rigor, respectively, to eliminate artifacts arising from resonance of tension transducers as reported previously (Kawai and Brandt, 1980).

The total power (T_{PWR}) of the force oscillation is:

$$T_{PWR} = \sum_{k=1}^{n-1} |F_k|^2. \tag{5}$$

F_n is not a part of the total power of force oscillation, because it is the average level of force and has nothing to do with the power. The relative amplitude of kth-order harmonic (RHA_k) is:

$$RHA_k = \frac{|F_k|}{\sqrt{T_{PWR}}}. \tag{6}$$

In particular, RHA_1 is called the linearity (Lin):

$$Lin = RHA_1 = \frac{|F_1|}{\sqrt{T_{PWR}}}. \tag{7}$$

This property is the same as the coefficient of correlation (or regression coefficient) when the time course data of force are fitted to the sinusoidal function, which is a linear fit. Eq. 2 is the result of the linear fit. The nonlinear amplitude (NLA) is:

$$NLA = \sqrt{\sum_{k=2}^{n-1} |F_k|^2}. \tag{8}$$

The nonlinear component of the complex modulus ($NLCM$) is:

$$NLCM = \frac{NLA}{L_1} = \sqrt{\sum_{k=2}^{n-1} |Y_k|^2}. \tag{9}$$

The nonlinearity (NL) is:

$$NL = \frac{NLA}{\sqrt{T_{PWR}}}. \tag{10}$$

Therefore,

$$Lin^2 + NL^2 = 1. \tag{11}$$

Note that all quantities defined in Eqs. 5, 6, 7, 8, 9, and 10 are functions of frequency (ν).

Solutions

The Na-skinning solution contained (in mM) 10 H_4EGTA, 7 Na_2H_2ATP, 2 $MgAc_2\cdot4H_2O$, 118 NaAc, and 10 MOPS. The K-skinning solution contained (in mM) 10 H_4EGTA, 7 Na_2H_2ATP, 2 $MgAc_2\cdot4H_2O$, 118 KAc, 48 KOH, and 10 MOPS. The standard Ca^{2+}-activating solution contained (in mM) 6 K_2CaEGTA, 12.1 Na_2H_2ATP, 11.5 $MgAc_2\cdot4H_2O$, 15 Na_2CP (creatine phosphate, CP), 2 KH_2PO_4, 2 K_2HPO_4 (4 total P_i), 1 NaAc, 53 KAc, and 10 MOPS; the pCa (= $-\log_{10}[Ca^{2+}]$) of this solution was 4.65, and [$MgATP^{2-}$] was 10 mM. The 0 mM phosphate (0P) Ca^{2+}-activating solution contained (in mM) 6 K_2CaEGTA, 6.1 Na_2H_2ATP, 6.4 $Mg(OH)_2$, 15 Na_2CP, 13 NaAc, 27 KAc, 11 KOH, and 10 MOPS; the pCa of

this solution was 4.55. The 30P Ca^{2+}-activating solution contained (in mM) 6 K_2CaEGTA, 5.9 Na_2H_2ATP, 6.7 $Mg(OH)_2$, 15 Na_2CP, 15 KH_2PO_4, 15 K_2HPO_4, 13 NaAc, 28 KAc, and 10 MOPS; the pCa of this solution was 4.52, and [$MgATP^{2-}$] was 5 mM. An intermediate P_i-activating solution was an appropriate mixture of 0P and 30P solutions. For fiber experiments, creatine kinase was added at 320 U/ml; creatine kinase was not used for myofibril experiments, because myofibrils were continuously exposed to a laminar flow containing fresh MgATP.

The relaxing solution contained (in mM) 6 K_2H_2EGTA, 7 Na_2H_2ATP, 2 $MgAc_2\cdot4H_2O$, 4 KH_2PO_4, 4 K_2HPO_4, 41 NaAc, 71 KAc, and 10 MOPS. The rigor solution contained (in mM) 4 KH_2PO_4, 4 K_2HPO_4, 55 NaAc, 122 KAc, and 10 MOPS. In the Ca^{2+}-activating and relaxing solutions, [Na^+] was 55 mM; [Mg^{2+}] was 1 mM; MgATP was 5 mM; ionic strength was 200 mM; and pH was adjusted to 7.00 using KOH. All experiments were performed at 15°C.

Online supplemental material

Fig. S1 shows a typical force time course record from a fully Ca^{2+}-activated myofibril experiment. Fig. S2 shows a typical force time course record from skinned muscle fiber experiments.

Results

The effect of P_i on tension and exponential processes

Fig. 1, A and D, shows active isometric tension; Fig. 1, B and E, shows stiffness (Y_∞); and Fig. 1, C and F, shows their ratio (tension/Y_∞) plotted against [P_i] (added concentration) in myofibrils (Fig. 1, A–C) and muscle fibers (Fig. 1, D–F) at 15°C. As expected from previous studies, tension and stiffness gradually decreased as [P_i] was increased from 0 mM to 30 mM. Their ratio remained in the range of 2.2%–3.3% L_O (Fig. 1, C and F), as previously reported with rabbit psoas skinned muscle fibers (Kawai and Halvorson, 1991; Caremani et al., 2008). Starting from 0 mM, the decrease in active tension was larger in myofibrils than in muscle fibers. For instance, comparing the 16 mM P_i point with the 0 mM P_i point, tension decreased by 58% in myofibrils (Fig. 1 A), whereas the decrease was 44% in muscle fibers (Fig. 1 D). This is because, when no P_i was added, there was an average of 0.7–0.8 mM P_i in muscle fibers (Kawai and Halvorson, 1991; Dantzig et al., 1992) owing to continuous hydrolysis of ATP, resulting in P_i accumulation and its diffusion across the cross-section of fibers. In myofibrils, the diffusion distance is almost negligible. Consequently, the data between 0 and 0.7 mM P_i are not included in the muscle fiber results of Fig. 1, D–F, where significant decrease in tension is observed (Fig. 1 A; Tesi et al., 2000).

Exponential process B (phase 3)

At each [P_i], sinusoidal analysis was performed, and the complex modulus data $Y(\nu)$ were collected. These data are plotted in Fig. 2 as Nyquist plots. Process B (called "oscillatory work," represented by the semicircle below the abscissa) is the largest at [P_i] = 30 mM; it decreases as [P_i] is reduced, and it disappears when [P_i] = 0 mM. Processes A and C, represented by two semicircles above the abscissa, are still present at [P_i] = 0.
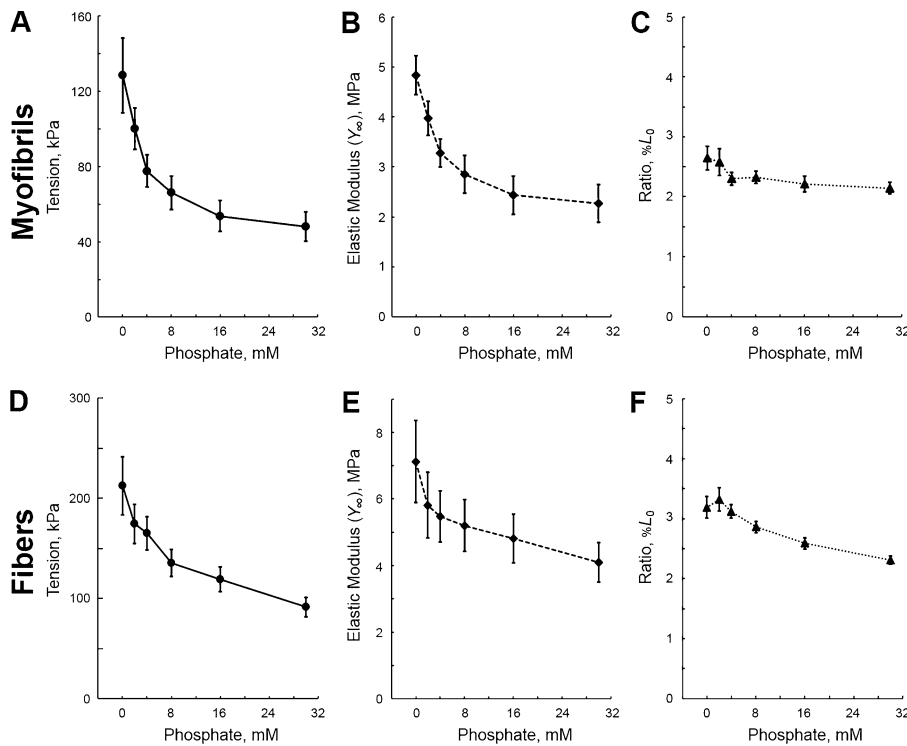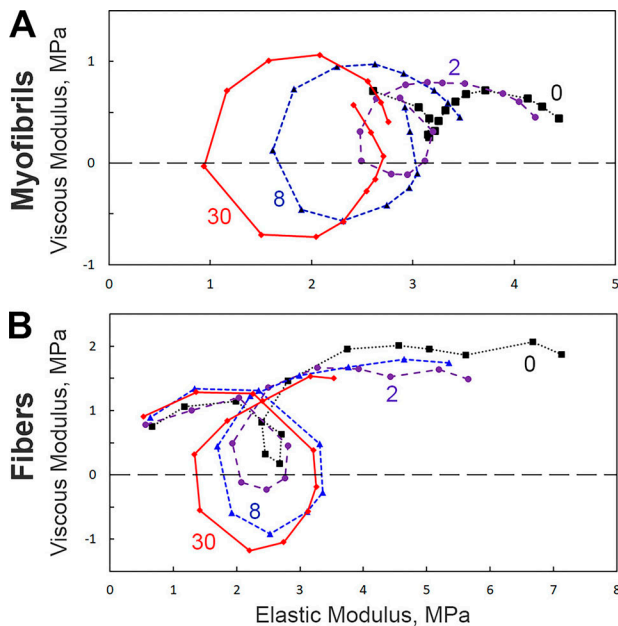
Figure 1. **Active tension and stiffness.** Active tension (in A and D), stiffness (elastic modulus, Y_∞, in B and E), and their ratio (tension/Y_∞ in C and F) are plotted against $[P_i]$. **(A–C)** Experiments with myofibrils ($n = 9$). **(D–F)** Experiments with muscle fibers ($n = 10$). Averages are shown with SEM (error bars).

Fig. 3 is a plot of the complex modulus $Y(\nu)$ as a function of frequency (ν) at six different $[P_i]$ values. Fig. 3, A and C, shows dynamic modulus ($|Y(\nu)|$) plots, and Fig. 3, B and D, shows phase shift $[\arg Y(\nu)]$ plots. Fig. 3, A and B, is from myofibrils (averaged for 12 preparations), and Fig. 3, C and D, is from muscle fibers

Figure 2. **Nyquist plots of the complex modulus data of active preparations.** These are plotted at four different $[P_i]$ values (0, 2, 8, and 30 mM as indicated; these are amounts of P_i added to the saline). **(A)** Myofibrils (average of 12 preparations). **(B)** Muscle fibers (average of 10 preparations). A decrease of exponential process B (central circular loop, in part with negative viscous modulus) as $[P_i] \to 0$ mM is seen in myofibrils (A) but not in fibers (B).

(averaged for 10 preparations). The changes in phase shift and dynamic modulus are larger at a higher $[P_i]$ because of larger oscillatory work production. The data of Fig. 3 were fitted to Eq. 4 (continuous curves) to deduce magnitudes and apparent rate constants of exponential processes A, B, and C. The resulting rate constant values are plotted in the logarithmic scale for myofibrils and muscle fibers in Fig. 4.

Our data, both in myofibrils and in fibers, show that with increasing $[P_i]$, the force response is delayed (lagged) behind the imposed length change, resulting in a larger negative phase shift at frequencies ~3–30 Hz at 30 mM $[P_i]$ (Fig. 3, B and D). A passive (ordinary) viscoelastic element only explains the positive phase shift ranging from 0° (pure elastic element) up to +90° (pure viscous element). Negative phase shifts indicate a delayed force in response to length change. This behavior is unexplained for passive viscoelastic elements and should underlie active processes of CBs that occur with frequencies near the characteristic frequency b. This negative phase shift (process B) is lost when $[P_i] \to 0$ (Fig. 3 B).

Exponential process C (phase 2)

In Fig. 3, a comparison of the experimental data (symbols) with those of theoretical curves (those fitted to Eq. 4) indicates that at frequencies ~30–100 Hz in phase shift plots (Fig. 3, B and D), the data fit better in myofibrils (Fig. 3 B) than in muscle fibers (Fig. 3 D). This means that process C is a purer monoexponential process in myofibrils than in muscle fibers. Process C is equivalent to phase 2 in step analysis (Table 1) of isometrically contracting fibers previously reported by other investigators, in which phase 2 of the force signal in step analysis was fitted to two exponential functions (Abbott and Steiger, 1977; Kawai and Zhao, 1993) or to four exponential functions (Ford et al., 1977),
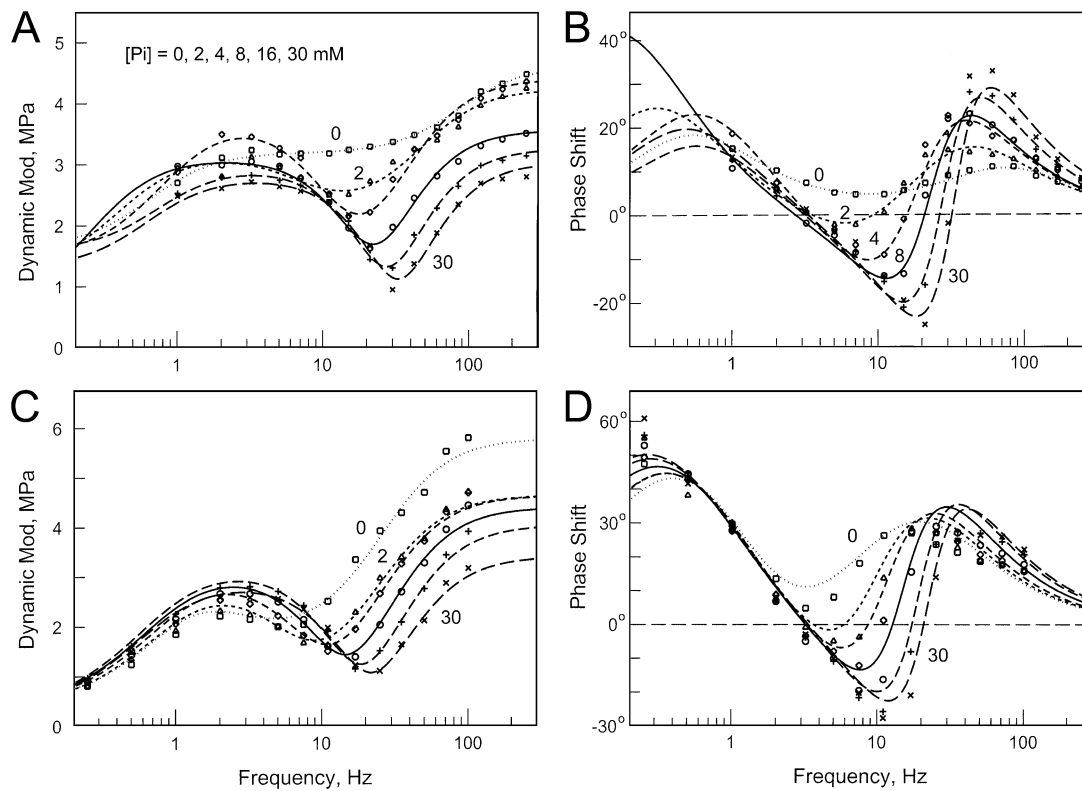
Kawai et al.
Phosphate effects in single myofibrils

Journal of General Physiology 6 of 16
https://doi.org/10.1085/jgp.202012755

Figure 3. Complex modulus (Mod) data $Y(v)$ of active muscle preparations. The data are plotted as a function of frequency at six $[P_i]$ values: 0 mM (open squares), 2 mM (filled triangles), 4 mM (open diamonds), 8 mM (open circles), 16 mM (+), and 30 mM (×). **(A and B)** Experiments with myofibrils averaged for 12 preparations. **(C and D)** Experiments with muscle fibers averaged for 10 preparations. A and C show dynamic modulus ($|Y(v)|$). B and D show phase shift (arg $[Y(v)]$). Smooth curves indicate best-fit data to Eq. 4. The complex modulus $Y(v)$ was first calculated at each frequency (v), then averaged for 10–12 preparations and plotted. This was essential because the data from individual preparations were noisy; to reduce the noise, averaging was performed.

thus considered to consist of distributed exponentials. Our results with myofibrils demonstrate that process C fits well to one exponential process, indicating that the elementary step of the
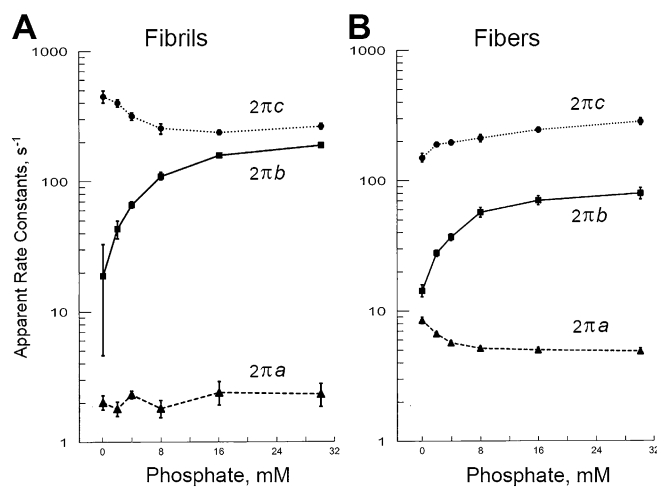

Figure 4. Effect of P_i on apparent rate constants. (A) Experiments with myofibrils averaged for 12 preparations. $Y(f)$ was averaged first, then fitted to Eq. 4 to find the apparent rate constants $2\pi a$, $2\pi b$, and $2\pi c$. **(B)** Experiments with muscle fibers for 10 preparations. The mean and SEM are shown, but most of the SEMs are smaller than the symbol size and cannot be seen.

CB cycle arising from this process can be approximated by a single-step chemical reaction, such as CB detachment (step 2) that follows ATP binding. In muscle fibers, this process may be blurred by mechanical factors such as residual intracellular membranes and desmin that link neighboring sarcomeres, as well as extracellular matrix components, including sarcolemma, collagen, and elastin (if present), causing the results of process C to appear as if the rate constant is distributed and does not exhibit a well-defined exponential function.

Effect of P_i on the apparent rate constant $2\pi c$

In myofibrils, the apparent rate constant $2\pi c$ decreased as $[P_i]$ was increased in the range of 0–16 mM and then slightly increased at 16–30 mM (Fig. 4 A). In muscle fibers, the initial decrease seen in myofibrils was absent, and then $2\pi c$ slightly increased (Fig. 4 B). $2\pi c$ was comparable between myofibrils and fibers for $[P_i]$ between 16 and 30 mM. To compare the relative effect of P_i on $2\pi b$ and $2\pi c$, Fig. 4 (log rate constants) should be used rather than Fig. 5 (linear rate constants). From Fig. 4, it is clear that the relative effect is much larger on $2\pi b$ than on $2\pi c$ in both muscle fibers and myofibrils. We interpret the biggest effect first, because, when the apparent rate constants are similar they interact with each other (Kawai and Halvorson, 1991; Kawai et al., 1993).

Competitive inhibition of the MgATP binding site by P_i

It was previously proposed that the apparent rate constant $2\pi c$ is associated with steps 1 and 2 (Scheme 1) of the CB cycle (Kawai, 1978; Kawai and Halvorson, 1989). Therefore, a decrease in $2\pi c$ as $[P_i]$ is increased in experiments with myofibrils (Fig. 4 A), suggesting competitive inhibition of MgATP binding by P_i, as shown in Scheme 1. This scheme (without competitive inhibition) is closely correlated with another proposed scheme that uses caged ATP to deduce kinetic constants (Goldman et al., 1984a, 1984b).

The apparent rate constant of Scheme 1 is formulated as in Eq. 12 (Kawai and Halvorson, 1989; Kawai and Halvorson, 1991):

$$2\pi c = \frac{K_1 S}{1 + K_i I + K_o D + K_1 S} k_2 + k_{-2}, \tag{12}$$

where I represents a competitive inhibitor, I is its concentration, and K_i is its inhibitory binding (association) constant to the MgATP site on myosin. ADP (MgADP) is released at the end of work performance; D is its concentration; and K_o is its binding constant to the ATP site of myosin. ATP is the substrate (MgATP), S is its concentration (5 mM in the current experiment), and K_1 is its association constant to the site. $K_1 = 2.9$ mM^{-1} was obtained earlier in myofibril experiments (Iorga et al., 2012); thus, $K_1 S = 14.5$. In Scheme 1 and Eq. 12, I can be any competitive inhibitor. The $2\pi c$ data were fitted to Eq. 12 by setting $I = [P_i]$ and $D < 0.02$ mM, $K_o = 2.8$ mM^{-1} (Kawai and Halvorson, 1989). Because $k_o D < 0.06 \ll 15.5$, the $K_o D$ term in Eq. 12 can be ignored. The result of fitting is plotted in Fig. 5. As seen in Fig. 5, the data fit well to Eq. 12, from which we deduced that $K_i = 0.38$ mM^{-1}. Thus, the inhibitory dissociation constant of P_i is $K_i' = 1/K_i = 2.6$ mM.

Effect of P_i on the apparent rate constant $2\pi b$

In the structured muscle system (fibers and myofibrils), the release of P_i is a reversible reaction step (Ulbrich and Rüegg, 1971; Webb et al., 1986) that occurs after externally adding P_i, which binds to actomyosin (AM)*·ADP intermediate and causes a shift of the equilibrium toward the AM·ADP·P_i state in Scheme 2. When the $[P_i]$ was increased from 0 to 30 mM, we observed that the apparent rate constant $2\pi b$ increased and approached saturation at high $[P_i]$ values (Figs. 4 and 6 A). $2\pi b$ was
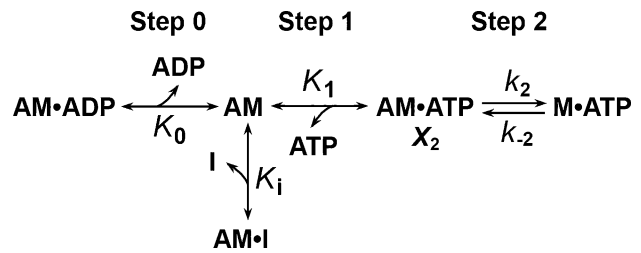
Scheme 1. **CB scheme surrounding ATP binding steps.** A, actin; M, myosin; I, inhibitor (competitive); X_2, [AM.ATP].

substantially larger in myofibrils than in fibers and spanned a larger range. In the higher concentration range (8–30 mM), $2\pi b$ and $2\pi c$ were closer in value in myofibrils than in fibers. Magnitude B also increased and approached a saturation at a higher $[P_i]$ (Fig. 6 B). Magnitude B extrapolated to 0 as $P_i \to 0$ mM, as seen in Figs. 2 and 6 B. Such an observation is consistent with the CB model depicted in Scheme 2, previously proposed for skinned fibers (Fortune et al., 1991; Kawai and Halvorson, 1991; Dantzig et al., 1992). At $[P_i] \to 0$ mM, along with the disappearance of the oscillatory work, frequency modulation of dynamic modulus, phase shift, and viscous modulus are all reduced (Fig. 3). This scheme is closely correlated with other schemes that used results from either caged P_i (Dantzig et al., 1992) or pressure-release experiments (Fortune et al., 1991) in muscle fibers. In each case, the kinetic constants obtained agree within a factor of 3.

The analytical form of the apparent rate constant in Scheme 2 is shown in Eq. 13, where $P = [P_i]$ (Kawai and Halvorson, 1991):

$$2\pi b = \frac{1}{1 + \frac{1}{K_3}} k_4 + \frac{K_5 P}{1 + K_5 P} k_{-4}. \tag{13}$$

With regard to the second intermediate, AM·ADP·P_i, in Scheme 2, CBs are in a weakly attached state, but at physiological ionic strength, AM·ADP·P_i is in fast equilibrium with M·ADP·P_i, during which CBs are detached. CBs in both detached and weakly attached states correspond to non–force-generating states, while the intermediates, AM*·ADP·P_i and AM*·ADP,
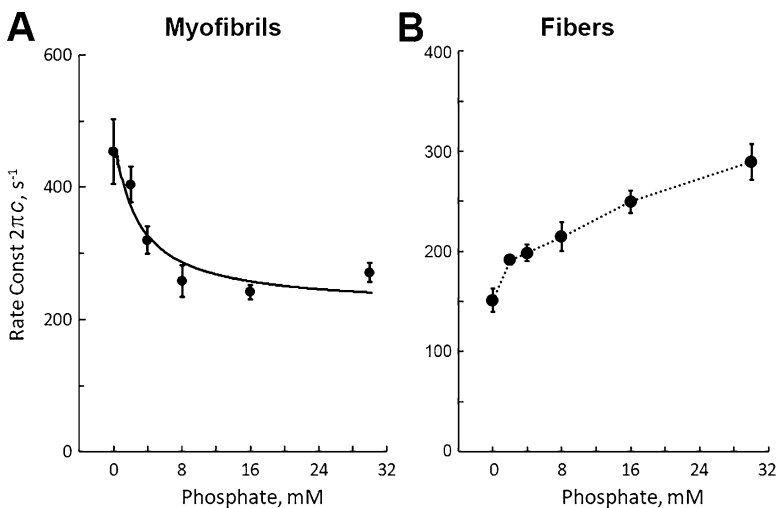
Figure 5. **The effect of P_i on the apparent rate constant (Const) $2\pi c$. (A)** Averaged myofibril data ($n = 14$) fitted to Eq. 12 with $I = [P_i]$. **(B)** Averaged muscle fiber data ($n = 10$). These are the same data as those shown in Fig. 4 in the logarithmic scale.

Kawai et al.
Phosphate effects in single myofibrils

Journal of General Physiology 8 of 16
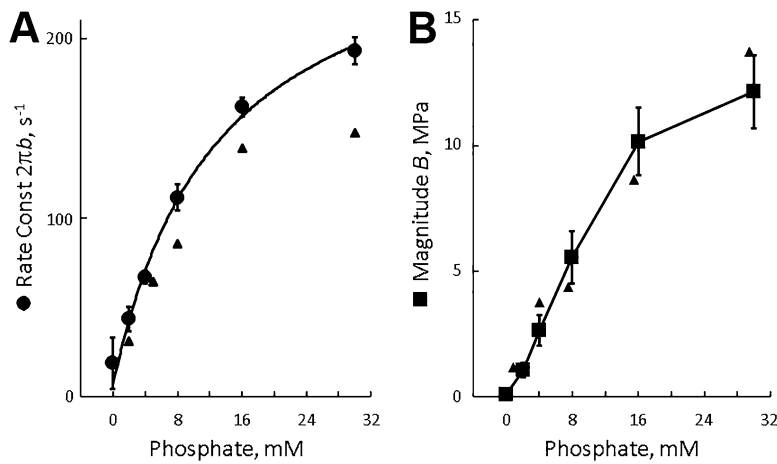https://doi.org/10.1085/jgp.202012755

Figure 6. **The effect of P_i on exponential process B in myofibrils, averaged for 14 preparations and plotted with SEM.** **(A)** Apparent rate constant (Const) $2\pi b$ (filled circles). The continuous curve is the best fit of the data to Eq. 13. **(B)** Magnitude B (filled squares). Averaged points are connected by straight lines. Small filled triangles in A indicate the peak (Fig. 7 D) position (ν_p) of the second harmonic amplitude; $2\pi\nu_p$ is entered here. Small filled triangles in B indicate the second harmonic amplitude (Fig. 7 D) at the peak position with baseline (0.06) subtraction and appropriate scaling (98×).

correspond to strongly attached force-generating CBs (Fortune et al., 1991; Kawai and Halvorson, 1991; Dantzig et al., 1992; Kawai and Zhao, 1993; Takagi et al., 2004). Our results with myofibrils are consistent with Scheme 2: Process B (oscillatory work) represents step 4, and its magnitude approaches 0 as $[P_i] \to 0$ mM. This demonstrates that CBs associated with AM·ADP·P_i and AM*·ADP·P_i intermediate states are required for oscillatory work production. From this fitting, in myofibrils, we obtained: $k_4/(1 + 1/K_3) = 7 \pm 9$ s^{-1}; $k_{-4} = 282 \pm 14$ s^{-1}; and $K_5 = 0.12 \pm 0.02$ mM^{-1} ($n = 14$). In muscle fibers, we found: $k_4/(1 + 1/K_3) = 19 \pm 2$ s^{-1}; $k_{-4} = 100 \pm 16$ s^{-1}; $K_5 = 0.11 \pm 0.02$ mM^{-1} ($n = 10$). That is, if $K_3 = 0.1$, then $k_4 = 77$ s^{-1} in myofibrils and $k_4 = 210$ s^{-1} in muscle fibers. However, the zero intercept has a large error in myofibrils (Fig. 6 A); thus, the k_4 value in myofibrils could not be determined with enough accuracy.

Little effect of P_i on the apparent rate constants $2\pi a$
The apparent rate constant $2\pi a$, corresponding to phase 4 in step analysis (Table 1), was noisy at 0–4 mM P_i and stable (but slightly increased) for 4–30 mM P_i in myofibrils (Fig. 4 A). In muscle fibers, $2\pi a$ decreased somewhat at 0–8 mM P_i and was stable for 8–30 mM P_i (Fig. 4 B). This difference might have been caused by the truncation of the measurement at 1 Hz in myofibrils. This truncation may also be the reason for the $2\pi a$ that is slower in myofibrils than in fibers (Fig. 4). The apparent rate

constant $2\pi a$ presumably corresponds to step 6 (Scheme 2: AM*·ADP → AM·ADP; ADP isomerization step), because it is similar to the ATP hydrolysis rate, and $k_6 \approx 2\pi a$ (Wang and Kawai, 2013).

Nonlinearity
After the steady state is achieved in 0.25 s, the tension time course is a repetitive function that can be expanded in a Fourier series (Eq. 2). The relative harmonic amplitudes were calculated from Eq. 6 and plotted for myofibrils (Fig. 7, A and B) and for muscle fibers (Fig. 7, E and F) for the activating condition at 8 mM P_i. Linearity (Lin; Eq. 7) is plotted in Fig. 7, A and E, and total nonlinearity (NL; Eq. 10) is plotted in Fig. 7, B and F. As seen here, Lin and NL appear to be the mirror image of each other because of the squared sum law (Eq. 11). These plots show that tension is most distorted at around ν_{min} (frequency that makes the dynamic modulus minimum), as reported previously in insect flight muscles (White and Thorson, 1972) and in rabbit psoas and crayfish walking leg muscle fibers (Kawai and Brandt, 1980). When the NLA (amplitude; Eq. 8) is plotted against frequency (Fig. 7 C) in myofibrils, this peak disappears, indicating that the apparent distortion is because $|Y_1(\nu)|$ is at the local minimum (at $\nu = \nu_{min}$; Fig. 3, A and C), which makes tension distortion (NL) appear large. NL is larger in myofibrils (Fig. 7 B) than in muscle fibers (Fig. 7 F; and as reported in Fig. 6 A of
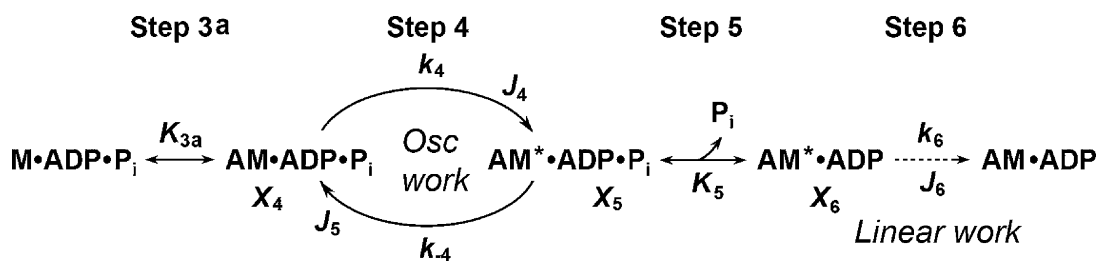
Scheme 2. **CB scheme surrounding the force generation and P_i release steps.** This scheme describes two types of work: oscillatory work and linear work. X_4, X_5, and X_6 represent the concentration of species shown above, such as $X_4 = $ [AM·ADP·P_i], $X_5 = $ [AM*·ADP·P_i], and $X_6 = $ [AM*·ADP]. J is the flux, defined by $J_4 = k_4X_4$, $J_5 = k_{-4}X_5$, $J_6 = J_4 - J_5 = $ ATP hydrolysis rate. Force generation occurs in step 4 and before P_i is released in step 5. Step 6 is the rate-limiting step and can be characterized by the ATPase rate. The essence of this scheme is based on three states (X_4, X_5, and X_6) and three kinetic constants (k_4, k_{-4}, and K_5), which can be measured with sinusoidal analysis combined with the P_i effect (Kawai and Halvorson, 1991). This scheme is also consistent with that measured by caged-P_i experiments (Dantzig et al., 1992) and pressure-release experiments (Fortune et al., 1991).
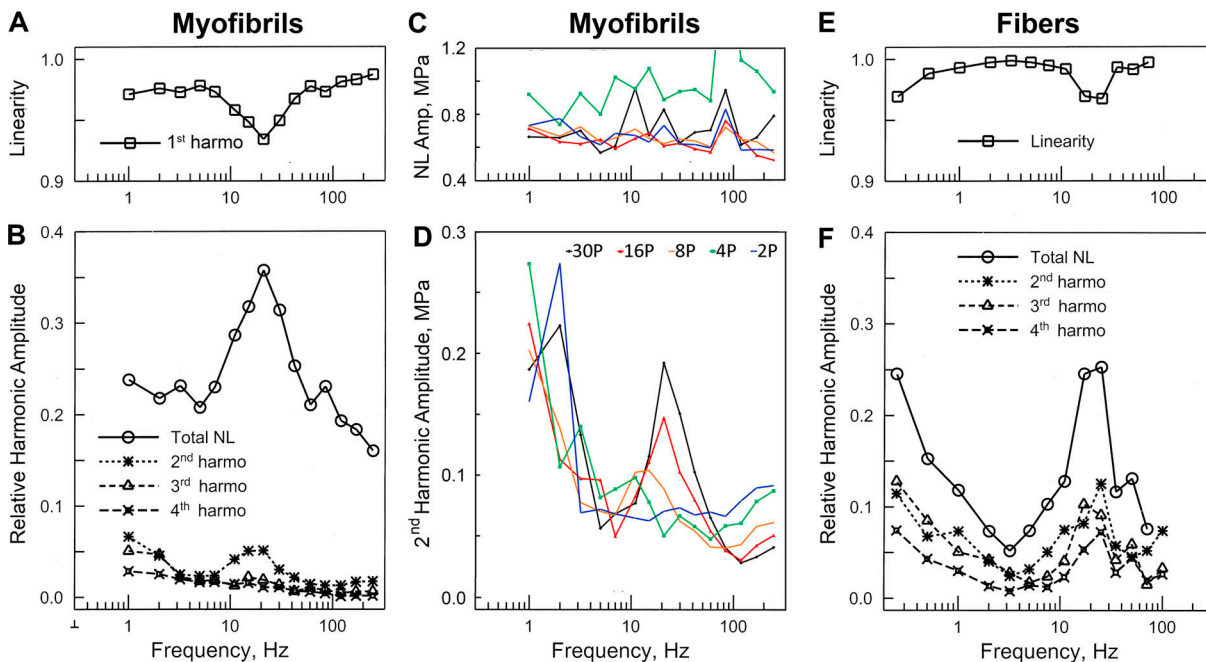
Figure 7. **Harmonic amplitudes. (A, B, E, and F)** Relative amplitudes of harmonic (harmo) components in force (Eq. 6) as functions of frequency in the 8 mM P_i solution. **(A and E)** Linearity (*Lin*; Eq. 7). **(B and F)** Nonlinearity (*NL*; Eq. 10) and relative amplitude of harmonic components $RHA_k(\nu)$ (k = 2, 3, 4; Eq. 6). **(C)** Total nonlinear amplitude (*NLCM*; Eq. 9) at five $[P_i]$ values as keyed at the top of D. **(D)** Amplitude of second harmonic component of the complex modulus ($|Y_2|$ in Eq. 3) at five $[P_i]$ values. A–D show the results of the myofibril study as averaged data (n = 14). E and F show the results of the muscle fiber study (n = 10).

Kawai and Brandt, 1980), primarily because the tension signal is noisier in myofibrils than in muscle fibers. Also plotted in Fig. 7, B and F, are the relative amplitudes of second through fourth harmonics, of which the second harmonic (*) is the largest and most significant.

The third and higher harmonics are smaller and presumably caused by the inherent white noise associated with myofibrillar tension measurements, which affects all frequencies similarly. In muscle fibers (Fig. 7 F), there is a hint of peaks at 17–25 Hz in third- and fourth-order harmonics; the low-frequency end has progressively larger *NL* because of a slow drift of the tension signal (note that the lowest frequency used is 0.25 Hz in fibers, whereas it is 1 Hz in myofibrils). The linearity (*Lin*) is the same as the relative amplitude of sinusoidal force response, whereas nonlinearity (*NL*) is its distortion amplitude including the noise. At 3 Hz in myofibrils, the sinusoidal amplitude in force is 0.98, whereas noise is 0.23. In contrast, in muscle fibers, the sinusoidal amplitude is 0.999, whereas noise is 0.05. This comparison indicates that the signal-to-noise ratio is four to five times larger in muscle fibers than in myofibrils, because force below the micronewton level must be measured in myofibrils compared with the millinewton-level force in muscle fibers. When $[P_i]$ is increased starting from 0 mM, the peak appears at ~25 Hz (Fig. 7, B and F) and reaches its maximum at 30 mM $[P_i]$ without changing other frequency data.

To examine the significance of the second harmonics, their amplitudes ($|Y_2|$; Eq. 3) are plotted in Fig. 7 D as functions of frequency for five different $[P_i]$ values (2–30 mM). A peak is observed in the midfrequency range (4–40 Hz). The peak is most prominent at the largest $[P_i]$, then gradually declines toward the

lower $[P_i]$, which is similar to the magnitude B (Fig. 6). To examine the significance of the correlation between the second harmonic and magnitude B, the peak frequency and peak value are entered in Fig. 6, A and B, respectively, in small filled triangles. These values were calculated from quadratic extrapolation of three points around the peak. These entries indicate a close correlation between oscillatory work (process B) and the second harmonic component, both in their rate constants and in their magnitudes. Similar analyses showed that the third or fourth harmonics were not associated with any exponential processes. In Fig. 7 D, second harmonics become noticeably large in the low-frequency range (1–4 Hz). This is caused by a slow drift in tension signal during the sinusoidal analysis, which becomes more significant at lower frequencies (Fig. 7 D) because a longer time is needed to collect the time course data. The linear drift was detrended, but the detrending was not fully successful, because the time course of the drift was not necessarily linear.

Discussion

Perturbation analysis

To observe the kinetics of force generation and P_i release steps in myofibrils or in muscle fibers, the first method is a change in the length of the preparation, the second is a change in $[P_i]$, and the third is a quick release in the pressure (Fortune et al., 1991), all of which perturbs the force generation step. For the first method, length change is either step or sinusoidal. For the second method, $[P_i]$ can be increased by photolysis of "caged P_i" as used in skinned fibers (Dantzig et al., 1992), or it can be changed by a solution switch as used in myofibrils (Tesi et al., 2000; Stehle

et al., 2002a). For the present study, we use the first method, a small-amplitude sinusoidal length change. These perturbations induce instability among CB states, and transient changes follow, enabling the detection of the kinetic constants of elementary steps, as shown in Schemes 1 and 2. With the first and third methods, $[P_i]$ is kept constant while the transient is induced by a length or pressure change. These methods are in general called "perturbation analysis methods" in which one of the extrinsic factors that influences a chemical reaction must be changed quickly but other factors must remain unchanged. It is important to emphasize that the speed of the change must be faster than the chemical reaction to be observed.

When the tension increase is large (such as during muscle activation), the concomitant tension time course is limited by the slowest step in the CB cycle (Gordon et al., 2000; Wang and Kawai, 2013), because several CB cycles must take place during force development to stretch the series compliance. The slowest step is also called the "rate-limiting step," which corresponds to the transition (step 6) in isometrically contracting muscles (AM*·ADP → AM·ADP) before ADP is released. When the tension decrease is large (during muscle relaxation), the concomitant time course may be influenced by the heterogeneous contraction and a propagation of a contraction wave (Stehle, 2017). We have employed small-amplitude sinusoidal length changes for two reasons: (1) this method does not require a large change in force and thus does not induce a heterogeneous contraction (Iorga et al., 2012), and (2) the length perturbation applied to each CB within the muscle/myofibrils is less than the power-stroke size. It is also important to note that this method covers a large frequency range, has a high resolving power, and is capable of resolving the elementary steps of the CB cycle as previously discussed (Kawai and Halvorson, 2007).

We have limited the frequency range to ≤250 Hz in myofibrils and ≤100 Hz in muscle fibers. This frequency range is adequate to characterize elementary chemical steps 2, 4, and 6 (processes C, B, and A, respectively; Fig. 4), which is the major focus of our study. This frequency range is in contrast to the stiffness measurement at 4 kHz, as reported previously (Caremani et al., 2008). While we were impressed to measure the stiffness at this high frequency, Caremani et al. reported little change in the tension:stiffness ratio as $[P_i]$ was changed. This is consistent with our data (Fig. 1, C and F) and earlier reports (Kawai and Halvorson, 1991), indicating that no new information is obtained, whether stiffness is measured at 4 kHz (Caremani et al., 2008) or extrapolated stiffness Y_∞ is used (current study). To characterize the properties of a viscoelastic material at a frequency as high as 4 kHz, it is preferable to measure stiffness, together with phase shift information, at frequencies such as 1, 2, 4, 8, and 16 kHz (for biopolymers) or using four additional frequencies between 1 and 16 kHz (for chemical reactions; see Fig. 3 for low-frequency example) to determine what was measured.

$[P_i]$ changes the number of CBs in the force-generating state, but it does not change force per CB
As $[P_i]$ was increased, both active tension and stiffness decreased similarly (Fig. 1, A and B), and their ratio remained

approximately constant (Fig. 1 C). While measured tension reflects the contribution of CBs in force-generating states, stiffness reflects the number of strongly attached CBs. Consequently, the tension:stiffness ratio reflects the force per CB. Therefore, the observations in Fig. 1 are consistent with Schemes 1 and 2, and they demonstrate that the population shift of CBs (reversal of steps 5 and 4 in Scheme 2) is the primary cause of tension decrease with increasing $[P_i]$ (Fig. 1 A). This conclusion is consistent with that of a previous study (Caremani et al., 2008). These inferences are implicit to the interpretations of earlier observations (Fortune et al., 1991; Kawai and Halvorson, 1991; Dantzig et al., 1992) and are actually shown to be the case in rabbit psoas fast-twitch fibers (Kawai and Zhao, 1993) and in rabbit soleus slow-twitch fibers (Wang and Kawai, 1997), but their significance was not explicitly stated.

The fact that $2\pi c$ is relatively insensitive to $[P_i]$ (Fig. 4; see also Kawai, 1986) demonstrates that there is not much signal coming from the force generation steps (step 4 and 5) in process C (phase 2). This insight is consistent with a previous study (Caremani et al., 2013) in which researchers found that $[P_i]$ did not have an effect on the rate constant r_2 of phase 2 during length transients of isotonically shortening psoas fibers. In contrast, a large effect of [ATP] on $2\pi c$ is consistent with the idea that process C (phase 2) represents both the ATP binding step and the subsequent CB detachment step (steps 1 and 2) in both myofibrils (Iorga et al., 2012) and muscle fibers (Kawai, 1978; Kawai and Halvorson, 1989). Unfortunately, there is no report that describes the effect of [ATP] on the rate constant r_2 measured on length transient during isotonic shortening, which is essential to determine whether r_2 is associated with the ATP binding and CB detachment steps. The fact that r_3 increases with $[P_i]$, as reported previously (Caremani et al., 2013), is consistent with our observation that $2\pi b$ increases with $[P_i]$ (Figs. 4 and 6 A; Table 1; see also Kawai, 1986) and demonstrates that phase 3 in step analysis (process B in sinusoidal analysis) is strongly influenced by the force generation step in the simple four-state model with four kinetic constants, as in Scheme 2. Thus, our model has a 1:1 correlation with experimental evidence. In contrast, previous investigators (Caremani et al., 2013) used a multistate model (with ≥24 states and 40 rate constants) to predict that phase 3 represents the CB detachment step, which appears to be more theoretical than experimental.

P_i as a competitive inhibitor of MgATP
Our study on myofibril mechanics demonstrates that P_i has a dual role: It reverses the P_i release step 5 (Scheme 2; Ulbrich and Rüegg, 1971; Webb et al., 1986), and, at the same time, it competitively inhibits ATP binding to the myosin head (Bagshaw and Trentham, 1974). We found that the inhibitory dissociation constant in psoas myofibrils is $K_i' = 1/K_i = 2.6$ mM. The binding site of the P_i molecule might be the P-loop (^{180}GXXXXGK^{185}T/S) of the myosin head, located at the ATP binding pocket in the 25-kD domain. This binding site is positively charged and normally captures the β and γ phosphates of the MgATP^{2-} molecule through Mg^{2+} chelation (Rayment et al., 1996). It is possible that either the negatively charged P_i^- or P_i^{2-} molecule neutralizes the positively charged P-loop, which

results in competitive inhibition. Previous authors (Bagshaw and Trentham, 1974; Amrute-Nayak et al., 2008) also reported that P_i competitively inhibited MgATP with $K_i' = 1.5$ mM in myosin subfragment 1 without actin. Another research group (Tesi et al., 1988) reported that both $P_i^{1.5-}$ and sulfate ions (SO_4^{2-}) bind to the ATP site with the inhibitory dissociation constant of 2.9 mM and 1.6 mM, respectively, at 100 mM KCl in a myofibril suspension. Other authors (Candau and Kawai, 2011) reported that P_i competitively inhibits MgATP binding with K_i' at 8 mM in myofibril suspensions. Thus, there is general agreement that the P_i ion binds to the nucleotide binding site of myosin and competitively inhibits MgATP binding. The reason why the same inhibitory effect is not seen in fibers is because $[P_i]$ <1 mM can hardly be achieved in fibers, whereas $[P_i]$ can approach 0.01 mM in myofibrils (Tesi et al., 2000), and the P_i inhibition effect can be seen most prominently at low-mM $[P_i]$ (Fig. 5). In addition, it is possible that because $2\pi c$ appears to be a distributed rate constant in fibers, a weak signal from the inhibitory effect is blurred in fibers. In contrast, process C is a clearly defined exponential process in myofibrils; hence, it can contain a weak signal from the inhibitory effect. Our earlier report shows a decrease of $2\pi c$ at low-mM $[P_i]$ in muscle fibers in different solution conditions (Kawai, 1986).

$[P_i]$ in skeletal muscle cells
In resting rat skeletal muscles (extensor digitorum longus and tensor fascia lata: fast-twitch type 2b), $[P_i]$ was measured at ~1.1–1.8 μmol/g (μmol/g is approximately mM), [CP] at 23–27 μmol/g, and [ATP] at 5.9–6.7 μmol/g using ^{31}P-NMR spectroscopy (Kushmerick et al., 1992). Our results show that $K_1 = 2.9$ mM^{-1}, $K_I = 0.38$ mM^{-1}, and $K_5 = 0.12$ mM^{-1}. Thus, at the start of contraction, $K_1[ATP] = 17$ and $K_I[P_i] = 0.57$; ATP binds to the ATP binding site 30 times more than P_i; hence, the inhibitory effect is negligible. Here, the isometric tension is at maximum (120 kPa; Fig. 1 A). During isometric contraction, $[P_i]$ may increase to 10 mM, in which case $K_I[P_i] = 3.8$, which is still 4.5 times less than ATP binding and might not be significant. When $[P_i] = 27$ mM (maximum concentration based on available [CP]), the binding of ATP is still larger than P_i, binding by 1.6 times. Thus, the effect of competitive inhibition by P_i to the ATP binding site might not be a problem under normal physiological conditions. The effect is seen simply because the phosphate group of ATP and P_i has the same steric conformation.

Fast-twitch muscles perform oscillatory work (Kawai and Brandt, 1980; Galler et al., 2005) that is stronger than that of slow-twitch muscles (Wang and Kawai, 1997; Kawai et al., 2018), although not as strong as that of insect flight muscles (White and Thorson, 1972). This implies that oscillatory work might be necessary for the fast movement of small rodents, particularly after exhaustion (during fatigue at the cellular level), when $[P_i]$ increases and isometric tension decreases concomitantly. It also implies that oscillatory work might not be essential for slow-twitch muscles used to maintain posture, particularly in large mammals. It would be intriguing to explore the molecular mechanism underlying oscillatory work in fast-twitch muscles in future research. Our earlier investigation has demonstrated that rabbit psoas fibers can be converted to an insect flight

muscle–type response simply by covalently cross-linking 22% of CBs to the thin filament (Tawada and Kawai, 1990).

Free energy change, force generation step, and P_i release step
In solution studies of purified and reconstituted contractile proteins, the AM*·ADP·P_i state was not recognized, and weakly bound AM·ADP·P_i goes directly to the AM*·ADP state (state without P_i), which is highly unidirectional: $K_5[P_i] << 1$, where K_5 is the association constant of P_i to CBs. This makes the step practically irreversible (10–100 M P_i is needed to reverse this step; Taylor, 1979), resulting in a large free energy reduction ($\Delta F = -RT \ln K_5[P_i]$). In solution, the liberated free energy is lost as heat to the surrounding medium. The large free energy reduction is the reason why the P_i release step (AM·ADP·$P_i \rightarrow$ AM*·ADP) has been considered to be the step that generates force (White and Taylor, 1976). However, the hyperbolic relation of $2\pi b$ to $[P_i]$ in our present study (Fig. 6 A), as well as in earlier studies by multiple investigating groups (Fortune et al., 1991; Kawai and Halvorson, 1991; Dantzig et al., 1992), indicates that the P_i release step actually consists of two steps, and it must be rewritten as: AM·ADP·$P_i \rightarrow$ AM*·ADP·$P_i \rightarrow$ AM*·ADP. These results are consistent with the hypothesis that force is generated during the first step and that the same force is maintained as P_i is released; this is true in fast-twitch fibers (Fortune et al., 1991; Kawai and Halvorson, 1991; Dantzig et al., 1992; Kawai and Zhao, 1993; Takagi et al., 2004) as well as in slow-twitch fibers (Wang and Kawai, 1997; Kawai et al., 2018). In myofibrils (Scheme 2; Fig. 6 B; and Tesi et al., 2000) and in fibers, the P_i release step is reversible (Ulbrich and Rüegg, 1971; Webb et al., 1986; Kawai and Halvorson, 1991; Dantzig et al., 1992), as evidenced by the fact that P_i has an effect on isometric tension (Fig. 1), and the rate constants behave as expected from Scheme 2 (Figs. 4, 5, and 6). Thus, the free energy changes of steps 4 and 5 are minimal to none. In myofibrils and muscle fibers, it must be that free energy liberated by ATP cleavage is stored as the potential energy (force) in the series elastic elements of the entire sarcomere (including the thick and thin filaments with myosin heads and associated proteins and the Z-line), thereby enabling the possibility of reversing the power stroke.

Oscillatory work and delayed tension
Process B has been known as oscillatory work with sinusoidal analysis (Pringle, 1967; Kawai et al., 1977; Kawai and Brandt, 1980) and as the rapid force recovery (phase 3) or delayed tension in step analysis (Pringle, 1967; Kawai, 1986; Davis et al., 2002) of skinned fibers. Process B has been interpreted to reflect the force generation step (Kawai and Halvorson, 1991; Kawai and Halvorson, 2007). The oscillatory work is shown by the area enclosed by the loop in the Nyquist plot (Fig. 2). This area is closed and clearly defined in Fig. 2 B, but it is not completely closed in Fig. 2 A because of the lack of data at frequencies <1 Hz. Production of the oscillatory work is not limited to the fourth quadrant in rabbit psoas because of the presence of processes A and C, which absorb work and compromise the oscillatory work produced. This loop diminishes and disappears as $[P_i] \rightarrow 0$; that is, $B \rightarrow 0$ (Figs. 2 and 6 B). At the same time, isometric tension (Fig. 1) and elastic modulus (Y_∞) assume their

maximal values. Previous studies on muscle fibers revealed that magnitude B was decreased by lowering the $[P_i]$, and the CB scheme was based on the assumption that $B \to 0$ when $[P_i] \to 0$ (Kawai and Halvorson, 1991; Kawai and Zhao, 1993). However, the significant accumulation of P_i (estimated to be 0.7 mM) in actively contracting fibers prevented the characterization of CB kinetics at near-zero $[P_i]$. Here, we present the sinusoidal analysis results for myofibrils in activating solutions with $[P_i]$ close to 0.

One important finding in our study is the complete loss of the magnitude of process B when no P_i is added to the activating solution in myofibrils (Figs. 2 and 6 B). However, we cannot exclude some residual P_i contamination (0.1–0.2 mM) in P_i-free solutions (Tesi et al., 2000; Stehle, 2017) because of continuous hydrolysis of ATP. However, this contamination is one-fifth of that estimated/measured in fibers (Kawai and Halvorson, 1991; Dantzig et al., 1992) or one-fifteenth of that predicted (~2 mM) on the basis of diffusion theory (Cooke and Pate, 1985) in activated muscle fibers. The loss of process B at low $[P_i]$, as now experimentally demonstrated in myofibrils, indicates that the P_i binding to the CB is essential for oscillatory work to be produced. Isometric tension increases as $[P_i] \to 0$ mM, because equilibria of Scheme 2 shift to the right and more CBs in force-generating states (AM*·ADP·P_i and AM*·ADP) accumulate, but force/CB does not change (Kawai and Zhao, 1993). Similarly, Y_∞ increases as $[P_i] \to 0$ mM, because the same equilibrium shift results in a larger number of strongly bound CBs at the AM*·ADP·P_i and AM*·ADP states. These pieces of evidence suggest that reversing the power stroke might be possible only in the presence of P_i in the structured muscle systems. Therefore, at physiological concentrations of P_i in contracting muscle cells, CBs can exit force-generating states by P_i rebinding (reversal of steps 5 and 4), in addition to the known path involving ADP release (step 0) followed by ATP binding to the myosin CBs (step 1).

Rate-limiting step

This part of the discussion is based on activated muscle that is held isometrically, as in the case of our experiments. If ATP binding (step 1 in Scheme 1) is rate limiting, then it follows that a change in [ATP] would result in no change in the apparent rate constants $2\pi b$ and $2\pi c$ or active tension, which is not supported by the data from ATP effect studies (Kawai, 1978; Kawai and Halvorson, 1989; Kawai and Zhao, 1993; Iorga et al., 2012). If CB dissociation (step 2) is rate limiting, then it follows that a decrease in [ATP] would result in an increase in the apparent rate constant $2\pi b$, which is not the case (Kawai and Zhao, 1993). If force generation (step 4) is rate limiting, then an increase in $[P_i]$ would diminish $2\pi b$, which is contrary to the data of Fig. 4 and Fig. 6 A. If P_i release (step 5) is rate limiting, $[P_i]$ should not affect the apparent rate constant $2\pi b$ or active tension, which is in contradiction to the data in Figs. 1 A, 4, and 6 A. If ADP isomerization (step 6, dashed arrow in Scheme 2) is rate limiting, then it follows that an increase in [ATP] results in increases of both $2\pi b$ and $2\pi c$, as observed (Kawai and Zhao, 1993; Iorga et al., 2012), and an increase in $[P_i]$ results in an increase in $2\pi b$, which is consistent with the data in Figs. 4 and 6 A and as reported (Kawai, 1986; Kawai and Halvorson, 1991). These increases will

also result in a decrease in active tension, as observed (Fig. 1). Consequently, we conclude that step 6 is the rate-limiting step for both isometrically contracting skinned muscle fibers and myofibrils from fast-twitch rabbit psoas muscles. In other words, identifying step 6 as the rate-limiting step is not an assumption in our CB model, but it is an established fact based on many lines of experimental evidence. Similar discussions were provided in our earlier publications (Kawai and Halvorson, 1989, 1991, 2007; Kawai and Zhao, 1993). The rate-limiting step in isotonically contracting muscle (without an imposed mechanical load) might be very different, as discussed previously (Nyitrai et al., 2006), because the kinetic constants associated with unloaded shortening muscle are considered to be very different from those associated with isometrically held muscles.

Distortion of tension sinewave associated with oscillatory work

It is interesting to note that the force sinewave (relative harmonic amplitude) is most distorted at ν_{min} (Fig. 7 B), the frequency at which $|Y(\nu)|$ assumes a local minimum, similar to earlier observations on insect muscles (Abbott, 1973; White and Thorson, 1972) and rabbit psoas and crayfish walking leg fast-twitch muscles (Kawai and Brandt, 1980). However, when the amplitude of nonlinear components (NLA) is plotted (Fig. 7 C; Eq. 8), the peak disappears. This means that there is distortion primarily because $|Y(\nu)|$ is small at around ν_{min}; hence, relative noise appears large. Apart from this, we were able to detect the second harmonic in the force sinewave ($|F_2|$ in Eq. 2), which has a local peak at ~20 Hz at 30 mM $[P_i]$ (Fig. 7 D). This peak is closely associated with oscillatory work (Fig. 6). The plots in Fig. 6 (small triangles) show that the peak frequency of the second harmonic amplitude ($|Y_2|$) is well correlated with the rate constant $2\pi b$ (Fig. 6 A), and that the peak value with magnitude B (Fig. 6 B). This observation indicates that the oscillatory work is intrinsically nonlinear and works against the forcing apparatus to modify the tension waveform. This can be explained as follows.

In Scheme 2, the process of oscillatory work is depicted within step 4. The flux of the reverse reaction is $J_5 = k_{-4}X_5$ (where $X_5 = $ [AM*·ADP·P_i]), which is consistent with our observation that oscillatory work (process B) disappears as $P \to 0$ (Figs. 2 A and 6 B). The flux of the forward reaction is $J_4 = k_4X_4$ (where $X_4 = $ [AM·ADP·P_i]), which is the force generation step in both fast-twitch (Fortune et al., 1991; Kawai and Halvorson, 1991; Dantzig et al., 1992) and slow-twitch (Wang and Kawai, 1997; Kawai et al., 2018) muscle fibers. The sinusoidal length change modifies J_4 and J_5 (oscillatory work), but presumably in an asymmetrical way. This is because $J_6 = J_4 - J_5 > 0$ (i.e., $J_4 > J_5$), where J_6 (related to the linear work) determines the ATP hydrolysis rate; the linear work results in sarcomere shortening. This difference between J_4 and J_5 becomes larger as the oscillation amplitude is increased, as demonstrated previously (Rüegg and Tregear, 1966) by measuring the ATP hydrolysis rate (J_6) on insect muscles. Thus, the length modulation of J_4 and J_5 is asymmetric in terms of stretch and release, which distort the force sinewave on the release side to result in an increased second harmonic as we have observed (Figs. 6 B and 7 D).

The stretch increases k_{-4} and decreases k_4, according to the Le Chatelier-Braun principle (Le Chatelier and Boudouard, 1898; Evans et al., 2001; Kawai and Halvorson, 2007); however, the effect of the change in length is not limited to the force generation step. It can also affect CB detachment (step 2) with the equilibrium constant K_2. Because step 2 is faster than step 4 ($c > b$), step 2 appears to be at equilibrium when step 4 is observed at around the characteristic frequency b. The stretch increases K_2 (Le Chatelier-Braun principle), which results in the increased probability of CBs in X_4, which in turn increases J_4.

In general, nonlinearity should be the unique phenomenon associated with the force-generating mechanism, as proposed previously (Huxley and Simmons, 1971; Huxley, 1974), because the length sensitivity of the forward and reverse rate constants are asymmetric to stretch and release. However, whereas they proposed that phase 2 (process C) is the force-generating step, it was later found to be the CB detachment step (step 2 in Scheme 1) on the basis of experimental evidence of the ATP effect (Kawai, 1978; Kawai and Halvorson, 1989; Kawai and Halvorson, 2007). Studies using caged ATP generally agree with Scheme 1 (Goldman et al., 1984a, 1984b). Furthermore, it was shown that phase 3 (process B) represents the force generation step on the basis of P_i effect (Kawai, 1986; Kawai and Halvorson, 1991; Kawai and Halvorson, 2007). Studies using caged-P_i and pressure-release methods closely agree with Scheme 2 (Fortune et al., 1991; Dantzig et al., 1992). Fig. 7, B and D, demonstrates that process B is more distorted than process C, which is consistent with our hypothesis that process B (equivalent to phase 3 in step analysis) reflects the force-generating step, and process C (equivalent to phase 2 in step analysis) does not. Available pieces of experimental evidence (Fortune et al., 1991; Kawai and Halvorson, 1991; Dantzig et al., 1992; Kawai and Zhao, 1993; Kawai, 2003) are in accord with this hypothesis.

Physiological significance
The intracellular concentration of P_i in resting fast-twitch skeletal muscle is ~1 mM (Kushmerick et al., 1992). Because [CP] is 23–27 mM, there is a possibility that [P_i] can reach this level. In this condition, isometric tension decreases, as shown in Fig. 1, A and D, and fast-twitch muscles can generate oscillatory work (augmented magnitude B; Fig. 3; see also Galler et al., 2005). It might be that this oscillation (step 4) can assist the contraction. At the same time, P_i binds to the ATP site competitively, where the CB may behave as a local rigor bridge, which would stiffen the elastic structure of the muscle.

Conclusions
In experiments with isolated myofibrils, we used a preparation that allowed us to achieve a condition near 0 mM [P_i], thus enabling us to rigorously evaluate the effect of P_i. Our study revealed that, in myofibrils, P_i also acts as a competitive inhibitor of ATP binding in addition to reversing the P_i release step after force generation. We further observed that process C closely fits to a pure exponential, whereas in fibers, process C has an appearance of distributed rate constants (Figs. 2 and 3). However, the noise level was higher in myofibrils than in fibers. We have shown that P_i affects the frequency-dependent modulation of the viscoelastic property of myofibrils and plays an essential role for process B (oscillatory work) in sinusoidal analysis by reversing the P_i-release step, as was found in isolated muscle fibers (Kawai, 1986; Kawai and Halvorson, 1991). In the absence of P_i, oscillatory work disappears, suggesting that a reversal of the power stroke is unlikely to occur. Therefore, the single path for CBs to leave force-generating states is only by ADP release and a new ATP binding to the myosin CBs (Schemes 1 and 2; Kawai and Zhao, 1993; Stehle and Iorga, 2010).

References
Abbott, R.H. 1973. An interpretation of the effects of fiber length and calcium on the mechanical properties of insect flight muscle. *Cold Spring Harb. Symp. Quant. Biol.* 37:647–654. https://doi.org/10.1101/SQB.1973.037.01.078

Abbott, R.H., and G.J. Steiger. 1977. Temperature and amplitude dependence of tension transients in glycerinated skeletal and insect fibrillar muscle. *J. Physiol.* 266:13–42. https://doi.org/10.1113/jphysiol.1977.sp011754

Amrute-Nayak, M., M. Antognozzi, T. Scholz, H. Kojima, and B. Brenner. 2008. Inorganic phosphate binds to the empty nucleotide binding pocket of conventional myosin II. *J. Biol. Chem.* 283:3773–3781. https://doi.org/10.1074/jbc.M706779200

Bagshaw, C.R., and D.R. Trentham. 1974. The characterization of myosin-product complexes and of product-release steps during the magnesium ion-dependent adenosine triphosphatase reaction. *Biochem. J.* 141:331–349. https://doi.org/10.1042/bj1410331

Bartoo, M.L., V.I. Popov, L.A. Fearn, and G.H. Pollack. 1993. Active tension generation in isolated skeletal myofibrils. *J. Muscle Res. Cell Motil.* 14:498–510. https://doi.org/10.1007/BF00297212

Brenner, B. 1988. Effect of Ca^{2+} on cross-bridge turnover kinetics in skinned single rabbit psoas fibers: implications for regulation of muscle contraction. *Proc. Natl. Acad. Sci. USA.* 85:3265–3269. https://doi.org/10.1073/pnas.85.9.3265

Candau, R., and M. Kawai. 2011. Correlation between cross-bridge kinetics obtained from Trp fluorescence of myofibril suspensions and mechanical studies of single muscle fibers in rabbit psoas. *J. Muscle Res. Cell Motil.* 32:315–326. https://doi.org/10.1007/s10974-011-9264-7

Caremani, M., J. Dantzig, Y.E. Goldman, V. Lombardi, and M. Linari. 2008. Effect of inorganic phosphate on the force and number of myosin cross-bridges during the isometric contraction of permeabilized muscle fibers from rabbit psoas. *Biophys. J.* 95:5798–5808. https://doi.org/10.1529/biophysj.108.130435

Caremani, M., L. Melli, M. Dolfi, V. Lombardi, and M. Linari. 2013. The working stroke of the myosin II motor in muscle is not tightly coupled to release of orthophosphate from its active site. *J. Physiol.* 591:5187–5205. https://doi.org/10.1113/jphysiol.2013.257410

Colomo, F., N. Piroddi, C. Poggesi, G. te Kronnie, and C. Tesi. 1997. Active and passive forces of isolated myofibrils from cardiac and fast skeletal muscle of the frog. *J. Physiol.* 500:535–548. https://doi.org/10.1113/jphysiol.1997.sp022039

Colomo, F., S. Nencini, N. Piroddi, C. Poggesi, and C. Tesi. 1998. Calcium dependence of the apparent rate of force generation in single striated muscle myofibrils activated by rapid solution changes. *Adv. Exp. Med. Biol.* 453:373–382. https://doi.org/10.1007/978-1-4684-6039-1_42

Cooke, R., and E. Pate. 1985. The effects of ADP and phosphate on the contraction of muscle fibers. *Biophys. J.* 48:789–798. https://doi.org/10.1016/S0006-3495(85)83837-6

Dantzig, J.A., Y.E. Goldman, N.C. Millar, J. Lacktis, and E. Homsher. 1992. Reversal of the cross-bridge force-generating transition by photo-generation of phosphate in rabbit psoas muscle fibres. *J. Physiol.* 451:247–278. https://doi.org/10.1113/jphysiol.1992.sp019163

Davis, J.S., C.L. Satorius, and N.D. Epstein. 2002. Kinetic effects of myosin regulatory light chain phosphorylation on skeletal muscle contraction. *Biophys. J.* 83:359–370. https://doi.org/10.1016/S0006-3495(02)75175-8

Evans, D.J., D.J. Searles, and E. Mittag. 2001. Fluctuation theorem for Hamiltonian systems: Le Chatelier's principle. *Phys. Rev. E Stat. Nonlin. Soft Matter Phys.* 63:051105. https://doi.org/10.1103/PhysRevE.63.051105

Ford, L.E., A.F. Huxley, and R.M. Simmons. 1977. Tension responses to sudden length change in stimulated frog muscle fibres near slack length. *J. Physiol.* 269:441–515. https://doi.org/10.1113/jphysiol.1977.sp011911

Fortune, N.S., M.A. Geeves, and K.W. Ranatunga. 1991. Tension responses to rapid pressure release in glycerinated rabbit muscle fibers. *Proc. Natl. Acad. Sci. USA.* 88:7323–7327. https://doi.org/10.1073/pnas.88.16.7323

Galler, S., B.G. Wang, and M. Kawai. 2005. Elementary steps of the cross-bridge cycle in fast-twitch fiber types from rabbit skeletal muscles. *Biophys. J.* 89:3248–3260. https://doi.org/10.1529/biophysj.104.056614

Goldman, Y.E., M.G. Hibberd, and D.R. Trentham. 1984a. Initiation of active contraction by photogeneration of adenosine-5′-triphosphate in rabbit psoas muscle fibres. *J. Physiol.* 354:605–624. https://doi.org/10.1113/jphysiol.1984.sp015395

Goldman, Y.E., M.G. Hibberd, and D.R. Trentham. 1984b. Relaxation of rabbit psoas muscle fibres from rigor by photochemical generation of adenosine-5′-triphosphate. *J. Physiol.* 354:577–604. https://doi.org/10.1113/jphysiol.1984.sp015394

Gordon, A.M., E. Homsher, and M. Regnier. 2000. Regulation of contraction in striated muscle. *Physiol. Rev.* 80:853–924. https://doi.org/10.1152/physrev.2000.80.2.853

Heinl, P., H.J. Kuhn, and J.C. Rüegg. 1974. Tension responses to quick length changes of glycerinated skeletal muscle fibres from the frog and tortoise. *J. Physiol.* 237:243–258. https://doi.org/10.1113/jphysiol.1974.sp010480

Higuchi, H., T. Yanagida, and Y.E. Goldman. 1995. Compliance of thin filaments in skinned fibers of rabbit skeletal muscle. *Biophys. J.* 69:1000–1010. https://doi.org/10.1016/S0006-3495(95)79975-1

Huxley, A.F. 1974. Muscular contraction. *J. Physiol.* 243:1–43. https://doi.org/10.1113/jphysiol.1974.sp010740

Huxley, A.F., and R.M. Simmons. 1971. Proposed mechanism of force generation in striated muscle. *Nature.* 233:533–538. https://doi.org/10.1038/233533a0

Huxley, H.E., A. Stewart, H. Sosa, and T. Irving. 1994. X-ray diffraction measurements of the extensibility of actin and myosin filaments in contracting muscle. *Biophys. J.* 67:2411–2421. https://doi.org/10.1016/S0006-3495(94)80728-3

Iorga, B., L. Wang, R. Stehle, G. Pfitzer, and M. Kawai. 2012. ATP binding and cross-bridge detachment steps during full Ca^{2+} activation: comparison of myofibril and muscle fibre mechanics by sinusoidal analysis. *J. Physiol.* 590:3361–3373. https://doi.org/10.1113/jphysiol.2012.228379

Kawai, M. 1971. Light diffraction studies of frog striated muscle fibers. Ph.D. dissertation. Section 5.3.3, Fig. 54. Princeton University, Princeton, NJ.

Kawai, M. 1978. Head rotation or dissociation? A study of exponential rate processes in chemically skinned rabbit muscle fibers when MgATP concentration is changed. *Biophys. J.* 22:97–103. https://doi.org/10.1016/S0006-3495(78)85473-3

Kawai, M. 1986. The role of orthophosphate in crossbridge kinetics in chemically skinned rabbit psoas fibres as detected with sinusoidal and step length alterations. *J. Muscle Res. Cell Motil.* 7:421–434. https://doi.org/10.1007/BF01753585

Kawai, M. 2003. What do we learn by studying the temperature effect on isometric tension and tension transients in mammalian striated muscle fibres? *J. Muscle Res. Cell Motil.* 24:127–138. https://doi.org/10.1023/A:1026093212111

Kawai, M. 2018. Mathematics needed to solve problems of contraction. *In* Biomechanics, Muscle Fibers, and How to Interface Experimental Apparatus to a Computer. Springer International Publishing AG, London, UK. 65–76. https://doi.org/10.1007/978-3-319-72036-4_5

Kawai, M., and P.W. Brandt. 1980. Sinusoidal analysis: a high resolution method for correlating biochemical reactions with physiological processes in activated skeletal muscles of rabbit, frog and crayfish. *J. Muscle Res. Cell Motil.* 1:279–303. https://doi.org/10.1007/BF00711932

Kawai, M., and H.R. Halvorson. 1989. Role of MgATP and MgADP in the cross-bridge kinetics in chemically skinned rabbit psoas fibers. Study of a fast exponential process (C). *Biophys. J.* 55:595–603. https://doi.org/10.1016/S0006-3495(89)82857-7

Kawai, M., and H.R. Halvorson. 1991. Two step mechanism of phosphate release and the mechanism of force generation in chemically skinned fibers of rabbit psoas muscle. *Biophys. J.* 59:329–342. https://doi.org/10.1016/S0006-3495(91)82227-5

Kawai, M., and H.R. Halvorson. 2007. Force transients and minimum cross-bridge models in muscular contraction. *J. Muscle Res. Cell Motil.* 28:371–395. https://doi.org/10.1007/s10974-008-9131-3

Kawai, M., and Y. Zhao. 1993. Cross-bridge scheme and force per cross-bridge state in skinned rabbit psoas muscle fibers. *Biophys. J.* 65:638–651. https://doi.org/10.1016/S0006-3495(93)81109-3

Kawai, M., P. Brandt, and M. Orentlicher. 1977. Dependence of energy transduction in intact skeletal muscles on the time in tension. *Biophys. J.* 18:161–172. https://doi.org/10.1016/S0006-3495(77)85605-1

Kawai, M., Y. Saeki, and Y. Zhao. 1993. Crossbridge scheme and the kinetic constants of elementary steps deduced from chemically skinned papillary and trabecular muscles of the ferret. *Circ. Res.* 73:35–50. https://doi.org/10.1161/01.RES.73.1.35

Kawai, M., T.S. Karam, J. Kolb, L. Wang, and H.L. Granzier. 2018. Nebulin increases thin filament stiffness and force per cross-bridge in slow-twitch soleus muscle fibers. *J. Gen. Physiol.* 150:1510–1522. https://doi.org/10.1085/jgp.201812104

Knight, P.J., and J.A. Trinick. 1982. Preparation of myofibrils. *Methods Enzymol.* 85(Pt B):9–12. https://doi.org/10.1016/0076-6879(82)85004-0

Kushmerick, M.J., T.S. Moerland, and R.W. Wiseman. 1992. Mammalian skeletal muscle fibers distinguished by contents of phosphocreatine, ATP, and Pi. *Proc. Natl. Acad. Sci. USA.* 89:7521–7525. https://doi.org/10.1073/pnas.89.16.7521

Le Chatelier, H., and O. Boudouard. 1898. Limits of flammability of gaseous mixtures. *Bull. Soc. Chim. Fr. (Paris).* 19:483–488.

Nyitrai, M., R. Rossi, N. Adamek, M.A. Pellegrino, R. Bottinelli, and M.A. Geeves. 2006. What limits the velocity of fast-skeletal muscle contraction in mammals? *J. Mol. Biol.* 355:432–442. https://doi.org/10.1016/j.jmb.2005.10.063

Poggesi, C., C. Tesi, and R. Stehle. 2005. Sarcomeric determinants of striated muscle relaxation kinetics. *Pflugers Arch.* 449:505–517. https://doi.org/10.1007/s00424-004-1363-5

Pringle, J.W. 1967. The contractile mechanism of insect fibrillar muscle. *Prog. Biophys. Mol. Biol.* 17:1–60. https://doi.org/10.1016/0079-6107(67)90003-X

Rassier, D.E., W. Herzog, and G.H. Pollack. 2003. Dynamics of individual sarcomeres during and after stretch in activated single myofibrils. *Proc. Biol. Sci.* 270:1735–1740. https://doi.org/10.1098/rspb.2003.2418

Rayment, I., C. Smith, and R.G. Yount. 1996. The active site of myosin. *Annu. Rev. Physiol.* 58:671–702. https://doi.org/10.1146/annurev.ph.58.030196.003323

Rüegg, J.C., and R.T. Tregear. 1966. Mechanical factors affecting the ATPase activity of glycerol-extracted insect fibrillar flight muscle. *Proc. R. Soc. Lond. B Biol. Sci.* 165:497–512. https://doi.org/10.1098/rspb.1966.0080

Stehle, R. 2017. Force responses and sarcomere dynamics of cardiac myofibrils induced by rapid changes in [P_i]. *Biophys. J.* 112:356–367. https://doi.org/10.1016/j.bpj.2016.11.005

Stehle, R., and B. Iorga. 2010. Kinetics of cardiac sarcomeric processes and rate-limiting steps in contraction and relaxation. *J. Mol. Cell. Cardiol.* 48: 843–850. https://doi.org/10.1016/j.yjmcc.2009.12.020

Stehle, R., M. Krüger, and G. Pfitzer. 2002a. Force kinetics and individual sarcomere dynamics in cardiac myofibrils after rapid ca^{2+} changes. *Biophys. J.* 83:2152–2161. https://doi.org/10.1016/S0006-3495(02)73975-1

Stehle, R., M. Krüger, P. Scherer, K. Brixius, R.H.G. Schwinger, and G. Pfitzer. 2002b. Isometric force kinetics upon rapid activation and relaxation of mouse, guinea pig and human heart muscle studied on the subcellular myofibrillar level. *Basic Res. Cardiol.* 97(Suppl 1):I127–I135. https://doi.org/10.1007/s003950200041

Sugi, H., T. Ohta, and T. Tameyasu. 1983. Development of the maximum isometric force at short sarcomere lengths in calcium-activated muscle myofibrils. *Experientia.* 39:147–148. https://doi.org/10.1007/BF01958866

Takagi, Y., H. Shuman, and Y.E. Goldman. 2004. Coupling between phosphate release and force generation in muscle actomyosin. *Philos. Trans. R. Soc. Lond. B Biol. Sci.* 359:1913–1920. https://doi.org/10.1098/rstb.2004.1561

Tawada, K., and M. Kawai. 1990. Covalent cross-linking of single fibers from rabbit psoas increases oscillatory power. *Biophys. J.* 57:643–647. https://doi.org/10.1016/S0006-3495(90)82582-0

Taylor, E.W. 1979. Mechanism of actomyosin ATPase and the problem of muscle contraction. *CRC Crit. Rev. Biochem.* 6:103–164. https://doi.org/10.3109/10409237909102562

Tesi, C., T. Barman, and F. Travers. 1988. Sulphate is a competitive inhibitor of the binding of nucleotide to myosin. A comparison with phosphate. *FEBS Lett.* 236:256–260. https://doi.org/10.1016/0014-5793(88)80326-0

Tesi, C., F. Colomo, S. Nencini, N. Piroddi, and C. Poggesi. 2000. The effect of inorganic phosphate on force generation in single myofibrils from rabbit skeletal muscle. *Biophys. J.* 78:3081–3092. https://doi.org/10.1016/S0006-3495(00)76845-7

Tesi, C., F. Colomo, N. Piroddi, and C. Poggesi. 2002. Characterization of the cross-bridge force-generating step using inorganic phosphate and BDM in myofibrils from rabbit skeletal muscles. *J. Physiol.* 541:187–199. https://doi.org/10.1113/jphysiol.2001.013418

Ulbrich, M., and J.C. Rüegg. 1971. Stretch induced formation of ATP-32P in glycerinated fibres of insect flight muscle. *Experientia.* 27:45–46. https://doi.org/10.1007/BF02137732

Wakabayashi, K., Y. Sugimoto, H. Tanaka, Y. Ueno, Y. Takezawa, and Y. Amemiya. 1994. X-ray diffraction evidence for the extensibility of actin and myosin filaments during muscle contraction. *Biophys. J.* 67: 2422–2435. https://doi.org/10.1016/S0006-3495(94)80729-5

Wang, G., and M. Kawai. 1997. Force generation and phosphate release steps in skinned rabbit soleus slow-twitch muscle fibers. *Biophys. J.* 73: 878–894. https://doi.org/10.1016/S0006-3495(97)78121-9

Wang, L., and M. Kawai. 2013. A re-interpretation of the rate of tension redevelopment (k_{TR}) in active muscle. *J. Muscle Res. Cell Motil.* 34: 407–415. https://doi.org/10.1007/s10974-013-9366-5

Webb, M.R., M.G. Hibberd, Y.E. Goldman, and D.R. Trentham. 1986. Oxygen exchange between Pi in the medium and water during ATP hydrolysis mediated by skinned fibers from rabbit skeletal muscle. Evidence for Pi binding to a force-generating state. *J. Biol. Chem.* 261:15557–15564. https://doi.org/10.1016/S0021-9258(18)66750-X

White, H.D., and E.W. Taylor. 1976. Energetics and mechanism of actomyosin adenosine triphosphatase. *Biochemistry.* 15:5818–5826. https://doi.org/10.1021/bi00671a020

White, D.C., and J. Thorson. 1972. Phosphate starvation and the nonlinear dynamics of insect fibrillar flight muscle. *J. Gen. Physiol.* 60:307–336. https://doi.org/10.1085/jgp.60.3.307

Zhao, Y., P.M.G. Swamy, K.A. Humphries, and M. Kawai. 1996. The effect of partial extraction of troponin C on the elementary steps of the cross-bridge cycle in rabbit psoas muscle fibers. *Biophys. J.* 71:2759–2773. https://doi.org/10.1016/S0006-3495(96)79469-9
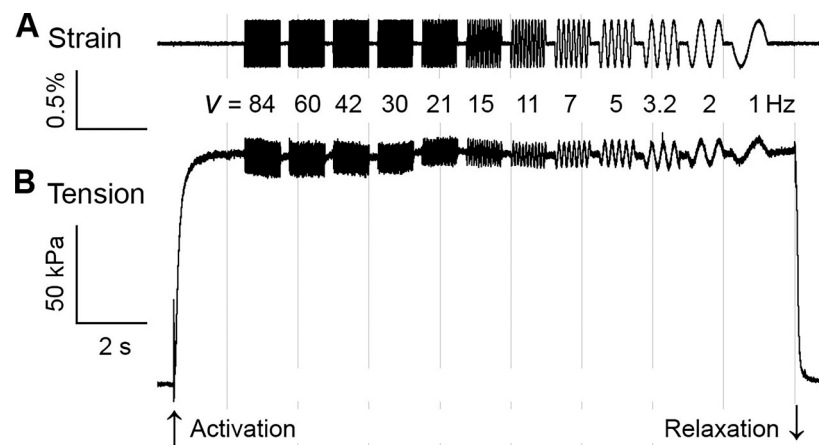
Supplemental material

Figure S1. **A typical force time course record from a fully Ca^{2+}-activated myofibril experiment. (A)** Length change (strain) with the amplitude of 0.2% L_0. Frequency (v) is shown in Hz underneath each oscillation. **(B)** Tension and its transients as recorded simultaneously (the data pair were collected in every 0.5 ms). When oscillation was stopped, and if the tension is different before and after the oscillation at each frequency, a linear detrend was applied to the tension time course during the oscillation before deducing all kinetic parameters.
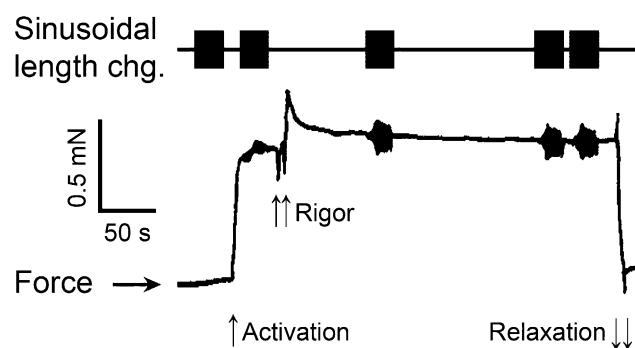

Figure S2. **A typical force time course record from skinned muscle fiber experiments.** The standard activation was followed by rigor induction. The timing of the sinusoidal length changes (chg.) is schematically represented on the top of the figure. The amplitude (strain) was 0.125% L_0 for all frequencies. The thickness of the pen trace represents the orifice size of the pen and not the noise. The force record was photographically reproduced from the original pen trace.